Streptococcus pneumoniae infection of lung epithelial cells induces internalization of surface GPI-anchored proteins through pneumolysin-mediated activation of host Rho GTPases

Nick Lee[1,#], Manmeet Bhalla [2,#], Joana M. Pereira[4,5,6], Stacie Clark [1,3], Sara E. Roggensack [1,3], Alenka Lovy[7], Michael J. Pereira[1,3], Guillermo Arroyo[1], Walter Adams[8], Andrew Camilli[1], Rodney K. Tweten[9], John M. Leong[1,10,*] Sandra Sousa[4,5,*] and Elsa N. Bou Ghanem[2,*]

[#]Co-first authors. *Co-corresponding authors. These authors contributed equally to this work.

[1]Department of Molecular Biology & Microbiology, Tufts University School of Medicine, Boston, MA

[2]Department of Microbiology & Immunology, University at Buffalo School of Medicine, Buffalo, NY

[3]Graduate Program in Molecular Biology & Microbiology, Tufts Graduate School of Biomedical Sciences, Boston, MA

[4]i3S-Instituto de Investigação e Inovação em Saúde, Universidade do Porto, Porto, Portugal

[5]Instituto de Biologia Molecular e Celular, Universidade do Porto, Porto, Portugal

[6]Molecular and Cellular (MC) Biology PhD Program, ICBAS - Instituto de Ciência Biomédicas Abel Salazar, University of Porto, Porto, Portugal

[7]Center for Vision Research and the Department of Ophthalmology and Visual Sciences, SUNY Upstate Medical University Syracuse, NY

[8]Department of Biological Sciences, San Jose State University, San Jose, CA

[9]Department of Microbiology & Immunology, The University of Oklahoma Health Sciences Center, Oklahoma City, OK

[10]Stuart B. Levy Center for the Integrated Management of Antimicrobial Resistance, Tufts University, Boston, MA

Running title: GPI-anchored proteins are internalized post pneumolysin intoxication.

Keywords: Pneumococcus, Lung Epithelial Cells, PLY, Glycosylphosphatidylinositol Anchored Proteins, GPI-AP, RhoGTPases, RhoA, Cdc42, Membrane Repair, Cholesterol-Dependent Cytolysins

*Please address correspondence to John M. Leong: John.Leong@tufts.edu, Sandra Sousa: srsousa@i3s.up.pt, and Elsa N. Bou Ghanem: elsaboug@buffalo.edu

Abstract

A return to homeostasis after infection-associated cellular injury can be accelerated by a rapid damage response. *S. pneumoniae*, a typically asymptomatic colonizer of the host upper respiratory tract, can cause serious and life-threatening infections when it gains access to the lungs and other organs. The cholesterol binding *S. pneumoniae* pore-forming toxin, pneumolysin (PLY), is central to the induction of host cell damage. Here, we first found that mouse lung infection by *S. pneumoniae* diminished pulmonary expression of CD73, a glycosylphosphatidylinositol anchored protein (GPI-AP) that modulates inflammation. Infection of the human pulmonary epithelial cell line H292 resulted in a PLY-dependent reduction of not only cell surface CD73, but also the population of surface expressed GPI-APs. The decrease in cell surface GPI-APs was rapid, required pore-forming activity, and could be recapitulated by purified PLY and other cholesterol binding cytolysins. In response to PLY-mediated insult, GPI-APs were not released from the surface of epithelial cells in extracellular vesicles but rather internalized by a mechanism dependent on the Rho GTPases RhoA and Cdc42. Internalization of GPI-APs was associated with lower levels of PLY-induced apoptosis and membrane permeabilization. These findings suggest that internalization of GPI-APs from epithelial cell membranes may constitute a rapid innate repair response to cell damage induced by PLY and other pore forming toxins that could help bacteria evade host defenses as many GPI-APs have roles in immunity.

Author summary

Streptococcus pneumoniae causes serious infections that can result in mortality. The pore-forming toxin, pneumolysin (PLY) produced by these bacteria is important for their ability to cause disease. Understanding how the host responds to damage by this toxin can result in better treatment against infection. In this study, we found that PLY-mediated injury results in decreased expression of glycosylphosphatidylinositol anchored proteins (GPI-AP) from the cell surface by internalization. GPI-AP co-localize in cholesterol-rich areas of the membrane where PLY inserts to form pores and cells with decreased surface GPI-APs were associated with less of PLY-induced cell death and membrane permeabilization. These results suggest that GPI-AP are internalized as part of repair mechanisms activated in response to infection-induced cell injury. As many GPI-APs have important roles in the immune response, their removal from the cell may inadvertently help the bacteria establish better infection.

Introduction

Streptococcus pneumoniae (pneumococcus), although an asymptomatic colonizer of the upper respiratory tract of healthy hosts, can, in susceptible populations, cause severe lower respiratory tract infections with high mortality and morbidity rates [1, 2]. *S. pneumoniae* predominantly causes pneumonia but can reach the bloodstream and cause serious extrapulmonary diseases, such as septicemia, meningitis, and endocarditis [3, 4]. More than 100 different *S. pneumoniae* serotypes have been identified based upon capsular polysaccharide content [5, 6], which plays a role in the severity of pneumococcal disease [7]. *S. pneumoniae* harbors many other virulence factors that promote its transition from the colonizer state to an infectious stage. These range from surface proteins involved in interaction with host pulmonary epithelium to the expression of factors that mediate metabolic adaptation or immune evasion [8].

Among these bacterial factors is a 53-kDa heat-labile cholesterol-dependent cytotoxin (CDC), pneumolysin (PLY), which is a highly conserved and important virulence factor that promotes the establishment of infection and evasion of host immune responses [9, 10]. PLY creates pores in the cell membrane [11-13] through a multistep process [14] in which 30-50 toxin monomers insert in the cholesterol-rich domains of host cells, oligomerize to form a large pre-pore complex [15, 16] that then undergoes conformational changes to produce a large 25-nm β-barrel pore in the membrane [11, 17]. Numerous studies have highlighted the role of PLY in damaging the pulmonary epithelium, activating the classical complement pathway, inducing inflammation, and inhibiting neutrophil function [8, 12]. Strains lacking PLY show reduced virulence [18].

Glycosylphosphatidylinositol-anchored proteins (GPI-APs) are expressed in highly divergent organisms, e.g., from protozoa to humans, and mediate diverse functions, such as environmental sensing, cell adhesion and migration, and immunomodulation [19-21]. GPI-APs are attached to the outer leaflet of the cell membrane through a highly conserved

118 glycosylphosphatidylinositol (GPI) anchor, which is composed of a phospholipid portion and a
119 glycan chain [22]. The GPI anchor is covalently linked to the C-terminus of the protein in a multi-
120 step post-translational modification process that occurs in the endoplasmic reticulum (ER) [23,
121 24]. The GPI-APs then migrates to the cell surface via the secretory pathway, which involves
122 trafficking through the ER, Golgi apparatus, and vesicular transport mechanisms, steps that are
123 at least partially dictated by the GPI anchor [25]. Machinery that controls membrane fusion and
124 sorting drives GPI-AP insertion in the plasma membrane, and in polarized epithelial cells, GPI-
125 APs are selectively sorted to the apical domain [26] where they are organized into lipid rafts,
126 specialized microdomains enriched in cholesterol and sphingolipids [22, 27]. In polarized cells the
127 clusters are assembled in the Golgi apparatus and traffic to the apical domain, while in non-
128 polarized cells the clusters organize from GPI-APs monomers already expressed at the cell
129 membrane [28]. The expression of GPI-APs on the cell surface is highly regulated. GPI-APs can
130 be released from the cell surface by the action of specific phospholipases, such as phospholipase
131 C (PLC) [20], which cleave the GPI anchor resulting in the release of the protein into the
132 extracellular environment. They can also be internalized through endocytosis, sorted and recycled
133 back to the cell surface following vesicular trafficking pathways [29].

134 Rho GTPases are small GTP-binding proteins that act as molecular switches by cycling
135 between an inactive GDP-bound state and an active GTP-bound state [30]. When activated, Rho
136 GTPases interact with downstream effector proteins to initiate specific signaling cascades, which
137 ultimately regulate key cellular functions [30]. In particular, Rho GTPases are implicated in the
138 regulation of intracellular membrane trafficking processes such as endocytosis, exocytosis, and
139 vesicle transport, and they control the cytoskeleton remodeling required for vesicle movement
140 and fusion with target membranes [31]. The Rho GTPase Cdc42 has been proposed as a
141 regulator of GPI-APs uptake [29]. During GPI-APs endocytosis, Cdc42 activation and the level of
142 cholesterol at the cell membrane are coupled, with concomitant recruitment of actin

143 polymerization machinery [32]. Following their internalization through a pathway that is
144 cholesterol-sensitive and dependent on Cdc42-activation, GPI-APs traffic to the recycling
145 endosomes and are recycled back to the cell surface, thus replenishing the pool of proteins that
146 may have been removed or degraded.

147 Many GPI-APs have roles in immune modulation [20, 24]. Among them is CD73, the
148 enzyme required for production of extracellular adenosine (EAD). EAD is produced in response
149 to cellular damage whereby the ATP released in the extracellular milieu is sequentially converted
150 to adenosine monophosphate (AMP) and then to adenosine by two surface ecto-nucleotidases,
151 CD39, a transmembrane protein and the GPI-AP CD73, respectively [33]. CD73 is crucial for host
152 resistance to infection by *S. pneumoniae* [34] as mice lacking this enzyme are highly susceptible
153 to infection and cannot control bacterial numbers [34]. We previously reported that the absence
154 of CD73 on neutrophils diminished their ability to kill pneumococcus [34], thus favoring bacterial
155 growth. Interestingly, the expression of CD73 is significantly reduced on neutrophils migrating into
156 the lungs in response to pneumococcal infection [35], indicating that pneumococcal infection may
157 result in the modulation of CD73 on host cell surfaces.

158 In this study, we report that infection with *S. pneumoniae* reduces CD73 surface
159 expression on host pulmonary epithelial cells. This reduction reflects a general effect of PLY on
160 the surface GPI-AP expression and depends on its pore forming capacity. The reduction in CD73
161 expression was not due to its release from the cell surface but rather due to internalization of GPI-
162 APs in a RhoA- and Cdc42-dependent manner. Internalization of GPI-APs was associated with
163 reduced host cell damage in response to PLY. This study identifies a possible mechanism through
164 which repair of damage caused by S*. pneumoniae* helps the bacteria potentially escape the host
165 immune response.

166

167

168 **Results**

169 **Infection with *S. pneumoniae* reduces the expression of GPI-APs on the surface of lung**
170 **epithelial cells.**

171 We previously found that the EAD-producing enzymes CD73 and CD39 were crucial for
172 host resistance against pneumococcal pneumonia [34, 36, 37]. To study the effect of *S.*
173 *pneumoniae* infection on the expression of CD73 and CD39, we intra-tracheally (i.t.) infected
174 C57BL/6 mice with *S. pneumoniae* TIGR4 strain or mock-treated with PBS. Forty-eight hours post
175 infection (hpi), the lungs were harvested and the expression of CD73 and CD39 on total lung cells
176 quantified using flow cytometry. *S. pneumoniae* significantly reduced the percentage of lung cells
177 that express CD73 compared to uninfected controls, while the expression of CD39 remained
178 unchanged (Fig 1A). In addition, a reduction in the amount of surface CD73 was detected on lung
179 epithelial ($EPCAM^+$) cells (Fig 1B).

180 To further explore the mechanisms involved, we modeled the decreased expression of
181 CD73 on lung epithelial cells *ex vivo* using H292 cells, a human pulmonary epithelial cell line
182 extensively used to study the interaction between the host factors and respiratory pathogens [38-
183 41]. Infection of H292 cells with increasing numbers of *S. pneumoniae* TIGR4 resulted in a dose-
184 dependent decrease in the expression levels of CD73 (Fig 1C), mimicking the *in vivo* finding.

185 These data indicate that *S. pneumoniae* infection specifically regulates the expression of
186 CD73, a GPI-AP, but does not affect the levels of CD39, a transmembrane protein [42]. We thus
187 tested if infection with *S. pneumoniae* selectively targets the surface expression of GPI-APs in
188 general. H292 cells infected with *S. pneumoniae* TIGR4 were labelled with antibodies recognizing
189 the GPI-APs CD55 and CD59 or stained with fluorescently labeled inactive variant of the protein
190 aerolysin (FLAER), which selectively binds GPI anchors at the cell membrane [43]. Flow
191 cytometric analysis showed that *S. pneumoniae* infection significantly reduced the expression of
192 both CD55 and CD59, as well as FLAER staining intensity (Fig 2A). This reduction was not

193 common to all surface proteins, as *S. pneumoniae* infection increased the expression of
194 transmembrane proteins such as CD47 and CD54 (Fig 2B). These findings indicate that
195 pneumococcus specifically reduces the surface expression of GPI-APs.

196 *In vivo*, epithelial cells are polarized, and GPI-APs mainly localize at the apical domain
197 [44]. To determine if the pneumococcus-induced reduction of GPI-APs surface exposure also
198 occurs on polarized epithelial cells, H292 cells were grown as polarized monolayers on Transwell
199 filters [39, 45]. The cells were then apically infected with *S. pneumoniae* TIGR4 for an hour and
200 the expression of GPI-APs was analyzed through flow cytometry. The expression levels of the
201 GPI-APs CD73, CD55 and CD59 were significantly reduced in infected cells as compared to the
202 uninfected controls (Fig S1). Overall, these data show that infection with *S. pneumoniae* reduces
203 the surface expression of GPI-APs on lung epithelial cells.

204 ***S. pneumoniae*-induced reduction of GPI-APs is dependent on the pore forming ability of**
205 **PLY.**

206 To determine if the reduced surface exposure of CD73 was strain dependent, H292 were
207 infected with D39, a serotype 2 strain of *S. pneumoniae*. Like TIGR4 infection, infection with D39
208 significantly reduced the expression of CD73 on H292 cells (Fig S2A), suggesting that the effect
209 of *S. pneumoniae* on CD73 surface expression is not strain specific. Infection of H292 cells with
210 Δ*cps* TIGR4, lacking the polysaccharide capsule, also reduced surface CD73 similarly to wild-
211 type TIGR4 (Fig S2A), thus indicating that the reduction of CD73 expression is independent from
212 the capsule. However, we found that heat-killed *S. pneumoniae* TIGR4 not only failed to reduce
213 CD73 expression on H292 cells but rather increased it (Fig S2B). This indicates that a heat-labile
214 bacterial factor is involved in reducing the expression of CD73 on lung epithelial cells.

215 *S. pneumoniae* pneumolysin (PLY) is heat-labile [12, 13], so we tested if the reduction in
216 CD73 is PLY-dependent. H292 cells infected with Δ*ply* TIGR4 did not show diminished CD73
217 expression on the cell surface compared to the uninfected controls (Fig 3A). Moreover, infection

218 of H292 cells with *Bacillus subtilis* expressing *ply* (*B. subtilis* PLY) significantly reduced levels of
219 CD73 as compared to cells challenged with wild-type *B. subtilis* (Fig 3A). To test if PLY alone is
220 sufficient for reducing the expression of CD73, H292 cells were treated with increasing
221 concentrations of purified recombinant PLY (rPLY). The expression of CD73 was reduced upon
222 incubation with rPLY in a dose-dependent manner (Fig 3A). Altogether, these findings
223 demonstrate that PLY is required and sufficient for decreasing CD73 from the cell surface of
224 pulmonary epithelial cells.

225 To determine if pore formation is required to decrease CD73 expression on host cell
226 surface, we tested PLY mutants defective at different stages of pore formation. 2.5 µg/ml of wild-
227 type PLY elicited more than 3-fold reduction in CD73 expression (Fig 3A and B) but the same
228 concentration of PLY ^{T456G}, which is incapable of binding cholesterol [46], PLY $^{M-1}$, which is locked
229 at an early stage of pore formation [11, 15, 47], or PLY $^{P-1}$, which is locked at late stage [11, 15,
230 47], failed to induce any change in CD73 expression on lung epithelial cells (Fig 3B). These results
231 indicate that the phenotype observed requires the pore-forming ability of PLY.

232 As PLY pores may result in the death of lung epithelial cells during infection [48, 49], we
233 tested if the reduced expression of GPI-APs could be a consequence of cell death. We tracked
234 cell death following infection with *S. pneumoniae* TIGR4 by measuring apoptosis and found that
235 infection resulted in rapid apoptosis of H292 cells (Annexin^{+}) as early as 10 minutes post-infection
236 (Fig S3A). This depended on PLY, as infection with Δ*ply S. pneumoniae* TIGR4 was not
237 associated with a significant effect on cell viability (Fig S3A). However, flow cytometric analysis
238 showed that infection with *S. pneumoniae* induced a similar significant 2-fold reduction in the
239 intensity of FLAER on both apoptotic (Annexin^{+}) and non-apoptotic (Annexin^{-}) cell populations
240 compared to the uninfected control groups (Fig S3B), demonstrating that decrease in GPI-APs is
241 not a result of cell death. We further confirmed that PLY-dependent reduction in GPI-APs could
242 be observed at this early 10-minute timepoint, as 10-minutes post-infection of H292 cells with

243 wild-type but not Δ*ply* TIGR4 resulted in significant reduction of FLAER binding (Fig 3C).
244 Altogether, these data indicate that *S. pneumoniae*-induced reduction in GPI-APs on host lung
245 epithelial cells is PLY-mediated.

246 **Cholesterol-dependent-cytolysins reduce the expression of GPI-APs at the surface of lung**
247 **epithelial cells.**

248 PLY belongs to a large family of cholesterol-dependent-cytolysins (CDC) that share
249 structural and functional properties [12]. To determine if the PLY-mediated reduction of GPI-APs
250 expression is a common feature shared among different members of CDCs, H292 cells were
251 challenged with two other CDCs: Streptolysin O (SLO) and Intermedilysin (ILY), produced by
252 Group A *Streptococci* and *Streptococcus intermedius*, respectively [50]. As pore formation is
253 required for reduction of GPI-AP expression, we treated H292s at concentrations sufficient to
254 induce equal levels of pore-formation, but that did not result in H292 cell death [11]. We found
255 that incubation of cells with SLO and ILY with 5 units of pore forming activity caused a reduction
256 in the FLAER intensity like that induced by PLY (Fig 3D), indicating that the decrease of GPI-AP
257 expression is a feature common to different CDCs.

258 **GPI-APs are not released from the cell surface upon infection with *S. pneumoniae*.**

259 GPI-APs can be removed from the host cell surface through cleavage by
260 phosphatidylinositol phospholipase C (PI-PLC) [51]. In fact, *S. pneumoniae* that produces the
261 pneumococcal surface protein C (PspC) can activate PI-PLC [52]. However, we found that PspC-
262 deficient *S. pneumoniae*, which are incapable of activating host PI-PLC, showed no defect in
263 triggering a reduction of surface CD73 (Fig S4A). In addition, treatment of H292 cells with the
264 phospholipase C specific inhibitor U-73122 (or its inactive analogue U-73343 [53]) did not
265 abrogate the *S. pneumoniae*-mediated reduction in CD73 surface expression (Fig S4B). These
266 findings indicate that reduction in cell surface associated CD73 upon *S. pneumoniae* infection
267 does not depend on the activity of host PI-PLC.

268 As part of a membrane repair mechanism, host cells infected with *S. pneumoniae* can
269 release extracellular membrane vesicles through which they expel membrane-bound bacterial
270 products such as PLY [54, 55]. To determine if CD73 was shed in host-derived vesicles, H292
271 cells were treated with CellTracker Green dye CMFDA, which stains the cell cytoplasm and can
272 be used to track host-derived vesicles. Following challenge with *S. pneumoniae* TIGR4, cell free
273 supernatants were collected, stained with FLAER and the presence of vesicles simultaneously
274 positive for FLAER and CMFDA was analyzed through flow cytometry. Surprisingly, we observed
275 a significant reduction in the percentage of vesicles FLAER$^+$ CMFDA$^+$ released by H292 cells
276 infected by *S. pneumoniae* compared to the uninfected controls (Fig S5), suggesting that the
277 decrease of GPI-APs induced by *S. pneumoniae* infection is not due to the release of extracellular
278 vesicles by the infected cells. As injured cells can also release parts of injured membranes via
279 the formation of protrusions named blebs [56, 57], we tested the effect of treating H292 cells with
280 blebbistatin, a drug reported to inhibit blebbing [58]. We found that treatment with blebbistatin did
281 not affect the levels of GPI-APs (Fig S6). Collectively, these data indicate that the reduction in
282 GPI-APs following pneumococcal infection is not due to their release from the cell surface by the
283 activity of phospholipases, shedding in vesicles or blebs.

284 **Infection with *S. pneumoniae* triggers the internalization of GPI-APs.**

285 As we found that the decreased levels of GPI-APs at the cell surface are not related to
286 their extracellular release, we tested if infection of lung epithelial cells by *S. pneumoniae* triggers
287 their internalization. To do so, H292 cells were infected with *S. pneumoniae,* stained with FLAER
288 to identify GPI-APs, and imaged by confocal microscopy. In conditions where H292 cells were
289 treated with HBSS (uninfected controls) or were challenged with Δ*ply S. pneumoniae*, GPI-APs
290 were uniformly detected on the surface of the cells (Fig 4A), following the outline of the cell
291 membrane. However, in *S. pneumoniae* infected cells, GPI-APs lose their uniform association to

292 the cell cortex and appear in clusters inside cells (Fig 4A, white arrows). These data suggest that
293 infection with *S. pneumoniae* triggers the internalization of GPI-APs.

294 If GPI-APs are removed from the cell surface by internalization (vs. extracellular
295 shedding), the total amount of GPI-AP associated with cells is predicted to be unchanged. To test
296 that, H292 cells were stained with FLAER before infection by *S. pneumoniae* ("PRE"). After 1 h,
297 cell-associated GPI-APs was quantitated by flow cytometry. Indeed, we found that FLAER
298 staining remained unchanged, i.e., was indistinguishable from FLAER staining of uninfected cells
299 (Fig. 4B, "PRE"). To confirm that under these experimental conditions, *S. pneumoniae* resulted in
300 the removal of GPI-APs from the cell surface, in parallel we stained H292 only after the 1 h
301 infection ("POST"). As predicted, surface staining by FLAER after infection revealed decreased
302 surface GPI-APs (Fig. 4B, "POST"). These findings confirm that infection with *S. pneumoniae*
303 induces the internalization of GPI-APs.

304 To test whether PLY was sufficient to trigger this process, as well as to follow GPI-AP
305 internalization in living cells, HeLa cells (chosen due to their ease of imaging by microscopy) were
306 pre-labelled with FLAER and then challenged with purified PLY or mock-treated. FLAER-stained
307 GPI-APs were visualized by fluorescent microscopy for 45 minutes (Supplementary video 1).
308 FLAER intensity was rapidly reduced on the cell surface upon challenged with PLY (Fig 4C and
309 Supplementary video 1), in addition FLAER signal was detected intracellularly within 3 minutes of
310 incubation with PLY (Fig 4C and Supplementary video 1) in structures resembling intracellular
311 vesicles (Fig 4C and Fig S7). At 45 min after PLY incubation FLAER signal at the surface of the
312 cells appeared to increase (Figure 4C and S7), suggesting that internalized GPI-APs are recycled
313 back to the cell surface. Overall, these data show that the infection with *S. pneumoniae* triggers
314 the internalization of surface GPI-APs which are then found intracellularly in vesicle-like
315 structures.

316 **Internalization of surface GPI-APs is mediated by PLY-induced activation of host Rho**
317 **GTPases RhoA and Cdc42.**

318 To explore the mechanism behind *S. pneumoniae*-mediated internalization of GPI-APs,
319 we first assessed a possible role of the actin cytoskeleton, given that dynamic changes in the
320 actin machinery are often required for endocytosis [59]. H292 cells were pre-treated with
321 Cytochalasin D, an inhibitor of actin polymerization, at 2 μM, a concentration that prevented the
322 actin-dependent cell-cell spread of *Listeria monocytogenes* ([60] and data not shown). Treatment
323 with Cytochalasin D did not affect the reduction of FLAER intensity following *S. pneumoniae*
324 infection (Fig S8A), suggesting an actin-independent mechanism for the internalization of GPI-
325 APs. Similar results were observed when Cytochalasin D pre-treated H292 cells were challenged
326 with PLY or SLO (Fig S8B), indicating that other CDCs also induce the internalization of GPI-APs
327 through a mechanism independent of actin polymerization.

328 The host Rho family of guanosine 5'-triphosphate (GTP)-binding proteins (GTPases) are
329 known to play important roles in protein trafficking, receptor-mediated endocytosis, and
330 internalization of GPI-APs [61]. To examine the role of Rho GTPases in the internalization of GPI-
331 APs induced by *S. pneumoniae* infection, H292 cells were treated either with *Clostridium difficile*
332 toxin B (ToxB), which irreversibly inactivates Rho GTPases by glucosylation [62], or with vehicle
333 control, before infection with *S. pneumoniae*. While infection with *S. pneumoniae* in vehicle-
334 treated cells caused the expected reduction in FLAER intensity indicating the decreased surface
335 expression of GPI-APs (Fig 5A), cell surface expression of GPI-APs was not affected in cells pre-
336 treated with ToxB (Fig 5A), suggesting a role for Rho GTPases in PLY-mediated GPI-APs
337 internalization. To confirm the role of Rho GTPases in the internalization of GPI-APs, we knocked
338 down their expression using RNAi. H292 cells were transfected with siRNAs targeting Cdc42,
339 RhoA and Rac-1 or with scrambled non-targeting siRNA as control. At 48 h post transfection, cells
340 were challenged with *S. pneumoniae* at a MOI of 10 for 1 h and FLAER intensity was quantified

341 through flow cytometry. Depletion of Cdc42 and RhoA but not Rac-1 abrogated the expected
342 reduction in FLAER intensity usually observed in H292 cells infected by *S. pneumoniae* (Fig 5B).
343 This indicates that the internalization of pneumococcal-mediated GPI-APs depends on the Rho
344 GTPases Cdc42 and RhoA.

345 Rho GTPases were previously reported to be activated by PLY in neuronal cells [13, 63].
346 We assessed if Cdc42 and RhoA are activated by PLY in epithelial cells in the time frame of PLY-
347 mediated internalization of GPI-APs. We transfected HeLa cells with plasmids encoding the
348 fluorescence resonance energy transfer (FRET) probes (CFP/YFP FRET pairs) that reflect the
349 activation state of RhoA or Cdc42. Each probe comprises a truncated form of the GTPase and
350 the Rho-binding domain (RBD) of effectors, bound to the CFP or YFP, respectively. The binding
351 of GTP to the GTPase (resulting in activation) brings the YFP-bound GTPase domain and the
352 CFP-bound RBD into close proximity, allowing FRET from CFP to YFP [55, 56]. Transfected HeLa
353 cells were challenged with 0.25 nM of PLY and live-cell microscopy was performed to visualize
354 the activation status of RhoA and Cdc42. FRET ratio (FRET/CFP) was calculated specifically at
355 the cell cortex using Image J. Cells were imaged for 20 min before PLY was added and for
356 additional 10 min after PLY challenge. For both probes, the ratio of FRET/CFP remained stable
357 during the 20 min before PLY addition, showing that the levels of GTPase activation do not vary
358 in these conditions (Fig 5C). Shortly after the addition of PLY, we observed a modest but
359 consistent increase in the FRET/CFP ratio levels. The increase detected for the Cdc42 probe was
360 very rapid and of short duration (about 40 s), while the increase for the RhoA probe appeared
361 more sustained in time (140s) (Fig 5C). These data suggest that PLY triggers a fast and transient
362 activation of both RhoA (Supplementary video 2) and Cdc42 (Supplementary video 3) at the cell
363 cortex. The ratio of FRET/CFP, for both probes, rapidly decreased to values that tended to be
364 lower than those obtained before PLY incubation (Fig 5C), indicating that although the activity of
365 RhoA and Cdc42 is triggered during the very early response to PLY induced damage, it is rapidly

366 shutdown. Overall, these data indicate that PLY induces internalization of GPI-APs through the
367 rapid, spatially, and temporally regulated activation of the Rho GTPases RhoA and Cdc42.

368 **GPI-APs are not required for PLY-mediated pore formation.**

369 The PLY-related CDC ILY utilizes the human GPI-AP CD59 as a receptor to induce
370 oligomerization and pore formation [64] and the cytolytic pore forming toxin aerolysin binds the
371 GPI moiety of the GPI-anchored T-lymphocyte protein Thy-1 [19]. To test whether PLY requires
372 the expression of GPI-APs on the host cell surface to form pores, H292 cells were either treated
373 with recombinant PI-PLC to cleave GPI-APs from the cell surface [51], or mock-treated with PBS.
374 As expected, treatment of cells with PI-PLC caused a significant reduction in the percentage of
375 GPI^+ cells ($FLAER^+$) compared to the untreated control group (Fig S9A). Upon addition of PLY to
376 H292 cells, we detected the expected decrease in GPI^+ cells compared to the untreated control
377 group (Fig S9A). We did not see a further reduction in the number of cells expressing GPI-APs
378 when PLY was added to PI-PLC pre-treated cells (Fig S9A).

379 We then assessed whether reduced expression of GPI-APs impact PLY-mediated pore
380 formation using PI permeability assays. We observed that PLY challenge induced a 4-fold
381 increase in the number of permeabilized cells (PI^+) in both the untreated and PI-PLC pre-treated
382 conditions in comparison to the respective baseline controls (Fig S9B). Finally, the average
383 intensity (MFI) of PI staining was unaltered by PI-PLC treatment. These data indicate that PLY
384 does not require surface GPI-APs to bind and form pores on host cell membranes.

385 **Internalization of GPI-APs is associated with lower levels of PLY-induced cellular damage.**

386 PLY forms pores in cholesterol rich domains, where GPI-APs are also colocalized [12].
387 Depending on the extent of damage, host cells can repair the damaged membrane and revert to
388 homeostasis [65]. To couple the kinetics of the PLY-mediated removal of GPI-AP from the cell
389 surface with an analysis of the population of cells that have undergone this reduction, H292 cells

390 were challenged with *S. pneumoniae* or mock-treated with PBS for different time periods and the
391 kinetics of reduction in FLAER intensity was determined throughout infection. According to our
392 previous live-cell imaging experiments of cells challenged with rPLY (Fig 4C), we expected the
393 reduction to occur rapidly. Indeed, *S. pneumoniae* significantly reduced FLAER intensity within
394 10 minutes of infection compared to the PBS-treated cells and retained this reduced level for the
395 remainder of the 90-minute observation period (Fig 6A). To analyze the specific population of
396 cells that reduced GPI-AP, we utilized flow cytometry and found that by 10 minutes after infection
397 approximately 60% of the infected cells showed reduced levels of GPI-AP (termed "GPI^{low}" cells)
398 (Fig 6B), a percentage that also remained stable through the rest of the experiment.

399 To test if the reduction of GPI-APs from the cell surface affected cellular viability, we
400 measured the staining of the population of GPI^{low} or GPI^{high} H292 cells by Annexin V, which stains
401 apoptotic cells, and PI, which stains cells with permeable membranes. Interestingly, we found
402 that, throughout infection, the population of infected GPI^{high} H292 cells had a significantly higher
403 percentage of membrane damaged (PI^{+}) (Fig 6C) and apoptotic (Annexin V^{+}) cells than the
404 population of GPI^{low} cells (Fig 6D). These findings suggest that reduced GPI-APs surface
405 expression is associated with reduced levels of PLY-induced damage. Altogether, these findings
406 suggest that cells with reduced expression of GPI-APs are more resistant to PLY-induced toxicity
407 and that the internalization of GPI-anchored proteins seems to be part of membrane repair that
408 limits the extent of PLY-induced cellular damage.

409

410

411

412

413

414 **Discussion**

415 The outcome of host-pathogen interaction is proposed to be mediated by the damage
416 response [66, 67]. This damage can be caused by the invading organism and/ or the host's
417 immune response to infection. *S. pneumoniae*, a typically asymptomatic colonizer of the host
418 upper respiratory tract, can cause serious and life-threatening infections when it gains access to
419 the lungs and other organs and this is directly linked to its ability to cause organ damage and
420 impair organ function [68-71]. One key component of this is the bacterial toxin PLY, found in all
421 the clinical isolates of *S. pneumoniae* [72]. PLY induces host cell damage by making pores in
422 cells [71]. However, host survival can be contingent on repairing/controlling infection-induced
423 damage [73]. In this study, we found that PLY-induced pores are associated with the rapid
424 removal of GPI-APs from the host cell surface, which can have profound effects on host response
425 to infection. PLY activated host RhoGTPases RhoA and Cdc42, resulting in the internalization of
426 GPI-APs (Figure 7). This internalization of GPI-APs was associated with reduced cellular damage
427 thus, suggesting the induction of host repair mechanisms.

428 GPI-APs are a heterogenous group of proteins which lack transmembrane domains and
429 are dependent on the GPI moiety for their expression on the cell surface [24]. Through their
430 interactions with the sphingolipids and cholesterol in the lipid bilayer, the GPI moieties anchor the
431 proteins in lipid-rich microdomains or membrane rafts [24, 74]. We found here that removal of
432 GPI-APs from the cell surface was not only mediated by PLY, but also occurred upon treatment
433 of host cells with other cholesterol dependent cytolysins (CDCs) including SLO and ILY. CDCs
434 bind to the cholesterol moieties in the host cell surface through the undecapeptide domain of the
435 peptide to mediate their cytolytic activity [14, 64]. Binding of the soluble monomeric form of the
436 CDCs to the cholesterol-rich membrane results in a sequence of structural changes causing
437 oligomerization of the monomers with subsequent formation of transmembrane β-barrel that
438 results in pore formation in the host cell membrane [64, 75]. Therefore, CDCs and GPI-APs will

439 likely localize together in cholesterol-rich microdomains at the cell surface where the damage
440 occurs. Consequently, internalization of GPI-APs following CDC-induced damage may be part of
441 membrane repair. Prior work with SLO showed that pores formed by the toxin are endocytosed
442 as part of the membrane repair process [76]. Here, we found that removal of GPI-APs by PLY
443 was dependent on the pore forming ability of the toxin and that internalization of GPI-APs was
444 associated with reduced cellular damage, suggesting that the host can repair the damage at the
445 membrane.

446 The type and extent of host cell damage as well as the host response to CDCs is highly
447 concentration dependent [65]. At high concentration levels, PLY induces irreversible loss of cell
448 membrane integrity and cellular homeostasis, while at lower concentrations, it activates host cell
449 repair mechanisms to restore their membrane integrity and to survive [65]. Initiation of host cell
450 repair of the plasma membrane depends on a limited influx of Ca^{2+} that triggers cytoskeletal
451 rearrangements to plug the holes in the plasma membrane [13, 77]. This has been described to
452 be mediated by the activation of host GTPases, re-localization of host intracellular organelles and
453 recruitment of cytoplasmic Ca^{2+} responsive proteins including annexins that interact with the
454 plasma membrane phospholipids at the injury site [13, 77, 78]. Host Rho GTPases, including Rho,
455 Rac and Cdc42, play a major role as molecular switches that regulate key cellular signaling
456 pathways and link surface receptors to the downstream processes culminating in endocytosis,
457 exocytosis and actin polymerization that affect cell polarity, migration, cytokinesis and vesicle
458 trafficking [79]. While exploring the cellular mechanisms that drive GPI-APs reduction at the cell
459 surface, we found that removal of GPI-APs from the cell surface upon *S. pneumoniae* infection
460 was dependent on Cdc42 and RhoA while Rac1 was not involved in this process. These data fit
461 with what has been reported in the literature regarding the role of Rho GTPases in the turnover
462 of GPI-APs under homeostatic conditions. GPI-APs are normally recycled from the cell surface
463 through an endocytic process called potocytosis involving caveolae, which is independent of both

464 dynamin and clathrin-mediated pathways [29, 80]. Once internalized, GPI-APs within the cell can
465 be seen in tubular structures called GPI-enriched endosomal compartments [80, 81].
466 Internalization of GPI-APs via endocytosis is under the regulation of host GTPases [80, 81]. This
467 includes CD59, one of the GPI-APs for which we observed reduction in surface expression upon
468 infection, whose internalization via endosomes is reported to be regulated by Cdc42 [82].
469 Additionally, perturbation in cholesterol moieties in the lipid bilayer also leads to internalization of
470 GPI-APs via clathrin-and dynamin-independent endocytic pathway [80]. Therefore, CDC binding
471 to the cell surface and pore formation results in the perturbation of the cholesterol rich
472 microdomains where GPI-APs are localized resulting in initiation of the endocytic pathway which
473 may lead to the repair of the injured membrane.

474 One of the interesting findings of this study was that actin polymerization had no apparent
475 role in the internalization of GPI-APs despite the activation of Cdc42 and RhoA. Cdc42 is a key
476 regulator of actin polymerization through the regulation of N-WASP and Arp2/3 complex and
477 similarly, RhoA also regulates actin polymerization [79]. Several recent reports have described
478 actin-independent endocytic events in various cell types. Work on non-adherent K562 human
479 erythroleukemic cells or adherent Cos-7 cells showed a lack of actin polymerization role in the
480 endocytosis process in these cells [83]. In another study, treatment of A431 cells (adherent and
481 in suspension) with cytochalasin D did not affect the process of endocytosis indicating an actin-
482 independent mechanism of endocytosis in these cells [83]. Additionally, the rational that the
483 polymerization of actin is important to generate the mechanical force required for vesicle fission
484 during clathrin-mediated endocytosis was recently challenged. In mouse chromaffin cells,
485 inhibition of dynamin GTPase but not of actin polymerization resulted in changes in the fission-
486 pore conductance in the endocytic membranes indicating that the pinching off of the endocytic
487 vesicle from the plasma membrane is actin-independent [84]. The requirement of actin in
488 endocytosis could be spatially regulated as in polarized cells inhibition of actin polymerization

489 blocked clathrin-mediated endocytosis from the apical but not the basolateral surface of polarized
490 Madin-Darby Canine Kidney Cells (MDCK) [85]. This study observed PLY-mediated reduction in
491 GPI-AP expression in pulmonary epithelial cells from infected murine models as well as in non-
492 polarized and polarized H292 cells. Overall, our findings point to a signaling pathway whereby
493 PLY activated Cdc42 and RhoA initiate internalization of GPI-APs independent of actin
494 polymerization machinery. Other bacterial pathogens have evolved to use actin polymerization-
495 independent mechanisms to trigger host responses. For example, *Salmonella enterica* serovar
496 Typhimurium was reported to activate Rho kinases to mediate entry into the cell by activating
497 myosin II independent of actin polymerization [86]. Similarly, *Listeria monocytogenes* was shown
498 to manipulate host exocytosis independent of actin polymerization to enter the host cell [87].

499 Apart from stimulating membrane repair through annexins, injury to plasma membrane by
500 PLY, LLO or SLO also results in a phenomenon called shedding whereby the host cell releases
501 extracellular vesicles to not only remove the injured part of the membrane but also to remove the
502 membrane bound toxin [54, 88]. Blebbing is one of the ways to mediate the shedding of larger
503 vesicular structures whereby the cell undergoes actomyosin-dependent localized contraction in
504 the plasma membrane to create confined spaces or a localized bulge with elevated Ca^{2+} levels to
505 prevent leakage to cytoplasmic contents and proteins in the extracellular milieu [13, 65]. These
506 localized bulges in the plasma membrane are eventually released by the cells either to remove
507 the areas of pores in case of a low degree of plasma membrane injury or to initiate the processes
508 of regulated apoptosis and inflammation in case of extensive cell damage [56, 65]. Since shedding
509 and blebbing result in the loss of part of the plasma membrane, it could also result in the loss of
510 expression of GPI-APs. However, data presented here using CMFDA dye to track the vesicles
511 and using chemical inhibition of blebbing showed that this was not the case. Surprisingly, we
512 observed a significant reduction in the percentage of vesicles FLAER+ CMFDA+ released by
513 H292 cells infected by *S. pneumoniae* compared to the uninfected controls. We also found no

514 evidence for the enzymatic release of GPI-APs from the cell surface to the extracellular milieu.
515 Certain bacterial species including *S. pneumoniae* have evolved to induce the expression of host
516 lipolytic enzyme phospholipase [89]. Given that the anchors of GPIs interact with the lipid moieties
517 of the plasma membrane, the GPI-APs are therefore susceptible to cleavage by phospholipases
518 [20, 21]. The findings here with phospholipase C specific inhibitor U-73122 and using a Δ*pspC S.*
519 *pneumoniae* strain showed that the reduction in CD73 expression following PLY treatment was
520 not a consequence of cleavage of GPI-APs by the host phospholipase.

521 The removal of GPI-APs from the host cell surface can seriously affect the host's ability to
522 control infection. These GPI-bound proteins are essential for many host physiological functions
523 including but not limited to enzymatic activities, nutrient uptake, complement regulators, immune
524 antigens and adhesion molecules [20, 28, 34, 90, 91]. This work shows that treatment with PLY
525 reduces CD55, CD59 and CD73 levels on pulmonary epithelial cells, all of which are GPI-APs
526 and important regulators of host inflammatory response. CD73 is an ectonucleosidase that is
527 required for initiating host responses to damage [42]. The host can sense infection-induced
528 damage by recognizing several damage-associated molecular patterns (DAMPS), including direct
529 recognition of extracellular ATP and its breakdown product adenosine in the extracellular
530 environment [92]. CD73 is required to dephosphorylate ATP, which has leaked from damaged
531 cells, into adenosine [93]. We previously found that extracellular adenosine production by CD73
532 was required for host resistance against *S. pneumoniae* in part by modulating epithelial responses
533 to these bacteria [34-36]. Other groups have also found that CD73 expression on epithelial cells
534 is important in other infections where CD73 expression on intestinal epithelial cells was needed
535 to control *Salmonella enterica* serovar Typhimurium infection [94]. Apart from CD73, both CD55
536 and CD59 act as inhibitors of complement membrane attack complex (MAC) [95, 96] and have a
537 role in neutrophil trans-epithelial migration [97]. Therefore, PLY's downregulation of CD55 and
538 CD59 could also have important implications on host immune responses. In summary, our

539 findings suggest that repair mechanisms activated in response to infection-induced cellular
540 damage may inadvertently help *S. pneumoniae* and other bacterial pathogens evade host
541 defenses, reflecting the dual function of PLY during infection.

542

543 **Materials and Methods**

544 **Ethics Statement:** Mice were handled in accordance with the recommended Guide for the Care
545 and Use of Laboratory Animals published by the National Institutes of Health. All procedures were
546 done according to the protocol approved by the University at Buffalo Institutional Animal Care and
547 Use Committee (IACUC), approval number MIC33018Y.

548 **Mice:** All the animal work was performed in 8-12 weeks C57BL/6J male mice purchased from
549 Jackson Laboratories (Bar Harbor, ME) and housed at a specific-pathogen free facility at the
550 University at Buffalo.

551 **Mammalian cell lines and media:** Human epithelial cervical cancer cell line HeLa (ATTC) and
552 pulmonary mucoepidermoid carcinoma cell line NCL-H292 (ATCC) were grown in Dulbecco's
553 modified Eagle's medium (ThermoFisher Scientific) and RPMI 1640 media (ThermoFisher
554 Scientific), respectively, supplemented with 10% fetal bovine serum (FBS) (ThermoFisher
555 Scientific) and 100 U penicillin/streptomycin (ThermoFisher Scientific). For all the experiments
556 involving lifting and/or seeding, the cells were washed twice with dPBS (Gibco) and treated with
557 Trypsin/EDTA (Gibco).

558 **Bacterial strains and growth conditions:** The following bacterial strains were used: *S.*
559 *pneumoniae* TIGR4 and D39 [98], PLY-deletion (Δ*ply*) [98], capsule-deletion (Δ*cps*) [99], and
560 pneumococcal surface protein C-deletion (Δ*pspC*) mutant strains of *S. pneumoniae* TIGR4 [100]
561 *B. subtilis* and its mutant expressing PLY (*B. subtilis* PLY) [101]. The pneumococcal strains were
562 grown to mid-log phase in Todd–Hewitt broth (BD Biosciences) supplemented with Oxyrase

563 (Fisher) and 0.5 % yeast extract at 37 °C/5 % carbon dioxide. Bacterial aliquots were then frozen
564 at –80 °C in growth media with 20 % glycerol. Tryptic Soy Agar plates with 5 % sheep blood
565 (Northeast Laboratory Services, P1100) were used to confirm the titers of *S. pneumoniae* in the
566 aliquots. Before infecting animals or H292 cells, bacterial aliquots were thawed and diluted in PBS
567 to the desired number. *B. subtilis* strains were grown overnight at 37 °C in Luria-Bertani (LB)
568 Broth.

569 **Toxin purification:** Purification of SLO (Streptolysin O), ILY (intermedilysin) and PLY (PLY) along
570 with its mutant forms was carried out as previously described [11, 47]. Briefly, the cultures of *E.*
571 *coli* BL-XL-1 Blue expressing polyhistidine-tagged toxins were grown in sterile TB broth (with
572 1:100 of overnight culture) grown at 37 °C with shaking at 200 rpm supplemented with 100 µg/mL
573 ampicillin. Expression of toxins was induced by the addition of isopropyl β-D-
574 thiogalactopyranoside (IPTG, Fisher Scientific) to a final concentration of 1 mM when the OD_{600}
575 of the culture reached 0.5-0.6 after which the cultures were allowed to grow overnight. This was
576 followed by centrifugation, resuspending and lysing bacterial pellets in PBS supplemented with
577 halt protease inhibitor cocktail (Thermo Fisher Scientific) using microfluidizer. The cell lysates
578 were centrifuged at 10000 g for 30 min at 4 °C and the clear supernatant was collected and
579 passed through Ni-NTA agarose column (Qiagen). Contaminating proteins were washed away by
580 passing a 20–120 mM imidazole gradient through the column while the bound toxins were eluted
581 using PBS containing 500 mM imidazole. The purity of the toxin was confirmed by running the
582 collected fraction on SDS-PAGE. The toxin-containing fractions were mixed with 10% (v/v)
583 glycerol and 5µM Tris(2-carboxyethyl) phosphine hydrochloride (TCEP) and flash-frozen on dry
584 ice and then shifted to −80 °C until use. *C. difficile* toxin B (Tox B) was purchased from Sigma.
585 Unless indicated, we used 0.25 nM of toxin for experiments with purified PLY as this concentration
586 corresponded to 1 pore forming Unit which causes PI uptake in only 50% of the cell population
587 and was sufficient to induce low-grade cellular damage.

588 **Toxin activity assay:** The activity of purified toxins was measured as previously described [11].
589 Briefly, aliquots of different toxins were thawed on ice and centrifuged at 14,000 rpm at 4 °C for
590 10 min to remove protein precipitates. Bradford assay (Bio-Rad) was used to measure the
591 concentrations of toxins per the manufacturer's instructions. Toxins at different concentrations
592 were added in wells of non-adherent 96-well plates containing approximately 1 x 10^5 H292 cells
593 and incubated for 10 min at 37 °C. Following incubation, cells were stained with propidium iodide
594 (PI) (1 mg/mL), incubated in dark at RT for 15 min and analyzed through flow cytometry. The toxin
595 concentration that caused permeabilization of 50 % of the H292 cells (PI+) was referred as "1
596 unit" (1U) of toxin activity. Cells treated with 5 % Triton X-100 acted as a positive control while
597 HBSS was used as negative control.

598 **Murine infection studies:** Mice anesthetized under isoflurane treatment were intratracheally (it)
599 instilled with *S. pneumoniae* TIGR4 at a dose of 2 x 10^6 CFU, as described previously [34, 102].
600 At 48 h post-infection, the mice were euthanized, lungs were harvested and single-cell suspension
601 was obtained by digesting the tissue in RPMI 1640 containing 10 % FBS and 2 mg/mL of type 2
602 collagenase (Worthington) and 30 µL/mL of 10 mg/mL DNase (Worthington) stock prepared in
603 dH_2O as previously described [102].

604 **Preparing heat killed *S. pneumoniae* TIGR4:** Frozen aliquots of *S. pneumoniae* TIGR4 were
605 thawed on ice, centrifuged at 1700 g for 5 min and resuspended in PBS in the original volume.
606 The bacterial suspension was then incubated at 65 °C for 2.5 h. Bacterial killing was confirmed
607 by plating the suspension on blood agar plate.

608 **Preparation of polarized H292 monolayers and infection with *S. pneumoniae*:** Polarized
609 H292 monolayers were prepared as previously described [45]. Briefly, the inverted side of the
610 filter membrane of 24-well Transwells with a pore size of 3 µm were coated with 70µL of 30µg/mL
611 of sterile collagen solution (3 mg/mL of collagen stock diluted in 60% ethanol) and allowed to dry
612 for 3 to 4 h at RT under sterile conditions. Approximately 1 x 10^6 H292 cells resuspended in RPMI

613 1640 media (with FBS and Pen/Strep) were added in the volume of 70μL on the coated filter
614 membrane and allowed to grow overnight at 37 ºC with 5 % CO_2. The following day, the Transwells
615 with cell were inverted into a sterile 24-well plate containing 1mL of H292 complete media and
616 cells were allowed to grow and polarize for a week at 37 ºC with 5 % CO_2. Cells were then washed,
617 infected apically with *S. pneumonia,* treated with trypsin and type II collagenase, stained for GPI-
618 APs, and analyzed by flow cytometry.

619 **Antibodies, inhibitors, and other reagents:** The antibodies used in flow cytometry studies to
620 measure the expression of specific GPI-APs included the following antibodies: anti-CD73 (AD2,
621 eBioscience), anti-CD39 (eBioA1, eBioscience), anti-CD55 (JS11, Biolegend), anti-CD47
622 (CC2C6, Biolegend) and anti-CD54 (HA58, Biolegend). The primary antibodies used for Western
623 blotting included anti-Rac1 (Proteintech) (1:1000), anti-Cdc42 (Cell Signaling) (1:1000), anti-
624 RhoA (Cell Signaling) (1:1000) and anti-GAPDH (MA5-15738) (1:5000). Horseradish peroxidase
625 (HRP)-conjugated secondary antibodies were purchased from Jackson Immunolabs. The
626 following anti-mouse antibodies were also used: Anti-CD326 (EpCAM) (G8.8, eBioscience), anti-
627 CD39 (24DMS1, eBioscience) and anti-CD73 (eBioTY/11.8, eBioscience). The inhibitors
628 Cytochalasin D, PI-PLC, PI-PLC inhibitor U-73122 and its control U-73343 (Invitrogen,
629 ThermoFisher Scientific) and Blebbistatin were purchased from Sigma and dissolved in DMSO
630 (unless indicated). As appropriate, control groups were treated with diluted DMSO, PBS or HBSS.

631 **Detection of plasma membrane integrity:** *S. pneumoniae* or PLY-induced cellular damage was
632 determined by using ANNEXIN/PI staining (BioLegend), per the manufacturer's protocol. Briefly,
633 infected H292 cells were centrifuged at 1200 rpm at 4 °C, the supernatants were discarded, and
634 pellets were re-suspended in 100 μL of Ca^{2+} free staining buffer (supplied with the kit). 2.5 μL of
635 FITC Annexin V and 5 μL of Propidium Iodide were used per sample. The samples were then
636 incubated for 15 min at room temperature (RT) in the dark and immediately analyzed by flow
637 cytometry.

638 **FLAER labeling:** Following challenge with different bacterial strains or toxins, H292 cells were
639 centrifuged at 1200 rpm at 4 °C, the supernatants were discarded, and pellets were re-suspended
640 in 50 µL of FLAER (FL2S, Cederlane) diluted in FACS buffer (HBSS Ca/Mg^+ containing 1% FBS)
641 at the final dilution of 1:100. The cells were then incubated for 30 min on ice in the dark. Following
642 incubation, the cells were washed twice with 100 µL of FACS buffer, resuspended in 300 µL of
643 FACS buffer and analyzed by flow cytometry.

644 **Flow cytometry:** Fluorescence intensities for different GPI-APs, Annexin V and Propidium Iodide
645 were measured on a BD Fortessa cytometer. At least 50,000 events for lung tissue and 10,000
646 events for *ex vivo* assays with H292 cells were captured for analysis. For the analysis of FLAER-
647 positive cell vesicles (Figure S5), the events were captured by legacy MoFlo cytometer. For the
648 data in Figure S9, the BD Accuri C6 flow cytometer was used to capture the events. All the
649 analysis was done using FlowJo software.

650 **RNA-interference:** Approximately, 1.5 x 10^4 H292 cells were seeded in 24-well plates (Falcon)
651 and cells were transfected the following day in serum free media using 100 nM of short interfering
652 RNA (siRNA), Opti-mem (Invitrogen) and the lipid reagent LF2000 (Invitrogen) as described
653 previously [1]. Serum was added on day 3 at a final concentration of 10% in the transfected wells.
654 On day 4, the cells were challenged with *S. pneumoniae* TIGR4 strain or lysed for Western blotting
655 to confirm protein depletion. SMARTpool siRNAs from Dharmacon were used to deplete Cdc42
656 (M-005057-01-0005), Rac1 (M-003560-06-0005) and RhoA (M-003860-03-0005). A non-
657 targeting NTC siRNA (D-001210-02-05) was used as a control.

658 **Western blotting:** To confirm protein depletion, approximately 48 h post-transfection H292 cells
659 were lysed on ice for 30 min in ice-cold RIPA buffer (1% Triton X-100, 0.25% sodium
660 deoxycholate, 0.05% SDS, 50 mM Tris-HCl [pH 7.5], 2 mM EDTA, 150 mM NaCl, 1 mM
661 phenylmethylsulfonyl fluoride, 1 mM sodium orthovanadate, 10 mg/liter each of aprotinin and
662 leupeptin), as previously described [103, 104]. The cell lysates were centrifuged at 12,000 rpm at

663 4 °C and bicinchoninic acid kit (Pierce) was used to determine the protein concentration in the
664 samples. An equal amount of protein (20 µg) was run on Mini-PROTEAN TGX Stain-Free Precast
665 Gels (BioRad) SDS-polyacrylamide gel and transferred to polyvinylidene difluoride (PVDF)
666 membranes. The membranes were blocked in 3% BSA for 1h at RT and incubated overnight at 4
667 °C with primary antibodies diluted in TBS/T with 3 % BSA. The membranes were washed thrice
668 with TBST (5 min per wash) followed by incubation with HRP-tagged secondary antibodies for 1
669 h at RT. The bands were detected using ClarityTM Western ECL substrate (BioRad) on the
670 ChemiDoc XRS+ system (BioRad).

671 **Measuring phosphatidylinositol-specific phospholipase C (PI-PLC) and PLY-induced cell**
672 **damage:** H292 cells were seeded in a 6-well plate (5 x10^5 cells/well) and 20 h later were pre-
673 treated with PI-PLC (0.1U) prepared in (Opti-MEM supplemented with 10mM Hepes, 1mM EDTA
674 and 0.1%BSA) [105]. Cells were then challenged for 10 min with PLY at 0.25 nM diluted in HBSS
675 (or HBSS only in the untreated condition). Cells were then harvested, centrifuged at 1200 rpm for
676 5 min at 4 °C and incubated for 30 min on ice in 50 µL of FACS buffer containing 0.5 µL of FLAER
677 (1:100). Following incubation, cells were washed and centrifuged at 1200 rpm for 5 min at 4° C
678 and resuspended in FACS buffer. Just before flow cytometry analysis, propidium iodide (PI) was
679 added at 2 ug/mL and incubated for 1 minute. Then, cells were analyzed for FLAER and PI
680 staining in BD Accuri C6 flow cytometer. At least 20,000 events per sample were collected. Data
681 obtained were analyzed using FlowJo software (Version 10.8).

682 **Immunofluorescence microscopy:** Approximately, 2 x 10^5 H292 cells were grown in a complete
683 medium on 13 mm diameter coverslips in 6-well plates. The day after, the cells were washed and
684 challenged with *S. pneumoniae* in serum-free RPMI 1640 medium. The plate was centrifuged at
685 1000 rpm for 2 min to enhance contact between bacteria and H292 cells and then incubated for
686 1 h at 37 °C in 5 % CO_2. Cells were washed in PBS, fixed in PBS with 4 % paraformaldehyde,
687 quenched with 20 mM NH4Cl (20 min), permeabilized with 0.1 % Triton X-100 (5 min) and blocked

688 with 3 % BSA in PBS (1 h). The antibodies were then diluted in PBS containing 1% BSA and cells
689 were labeled for GPI-AP nucleus and F-actin. GPI-AP using FLAER-Alexa 488 (Cedarlane)
690 (1:50), DAPI (Sigma) (1:1000) and Alexa fluor 680 phalloidin (Life technologies) (1:50),
691 respectively as described previously [106]. Cells were then washed and mounted with Vectashield
692 (Vector laboratories) and imaged using a 63 x 1.4 NA objective lens on a confocal laser-scanning
693 microscope (Leica SP8) and processed using ImageJ software.

694 **RhoA and Cdc42 activation and FRET:** HeLa cells seeded in Ibitreat 8-well dishes (4 x 10^4
695 cells/well) (Ibidi) were transfected approximately 20 h later with 300 ng of plasmid encoding FRET
696 probes (CFP/YFP FRET pairs) for RhoA or Cdc42 using jetPrime transfection reagent (Polyplus)
697 and incubated for 16–20 h to allow the expression of the recombinant proteins. FRET probes
698 used were described in [107, 108]. Cells were then kept in Opti-MEM (Gibco, without phenol red)
699 at 37 ℃ in 5 % CO_2 and imaged using Nikon TI microscope coupled with IRIS9 camera and using
700 60 x 1.4 NA objective. Cell imaging was started 20 min before PLY (0.25 nM) addition and
701 continued for 10 min after challenge with the toxin. CFP/FRET/YFP fluorescence data were
702 acquired after every 20 s. Image sequences were analyzed using ImageJ and FRET/CFP signal
703 ratio were calculated only at the cell cortex using a custom-made macro. A total number of 79
704 cells from 2 independent experiments were analyzed for RhoA activation and 74 cells were
705 analyzed from 2 independent experiments for Cdc42 activation.

706 **Live cell imaging and signal quantification:** HeLa cells were seeded in 8-well Ibidi plates
707 (1x10^5 cells/well) and 20 h later stained with FLAER (1:100) for 30 min. Cells were then imaged
708 using a Nikon Ti microscope coupled with IRIS9 camera with 40x 0.95 NA objective, for 15 min
709 with a time interval of 30 s before the addition of PLY (0.25 nM diluted in HBSS) or HBSS (used
710 as untreated control), and then for additional 45 min post PLY addition. Quantification of the
711 FLAER signal was obtained by image analysis using ImageJ. A total of 53 cells were analyzed.
712 The mean fluorescence intensity (MFI) was determined overtime in randomly selected regions of

713 interest (ROIs) at the cell membranes. These values were then normalized to the mean MFI
714 obtained from the same cells before these were challenged with PLY or HBSS.

715 **Statistical analysis:** Graph Pad Prism9 was used to perform all the statistical analysis. All the
716 data graphs represent the mean values +/- standard deviation (SD). Significant differences were
717 determined using One-way ANOVA followed by Tukey's or Dunnett's multiple comparison test or
718 Student's t-test or one sample t and Wilcoxon test, as indicated. *p* values of 0.05 or lower were
719 considered significant.

720

721 **Acknowledgements**

722 We want to thank Mafalda Sousa (ALM facility, i3S) for developing the macro for calculation of
723 the FRET/CFP signal ratio.

724

725 **Conflict of interest**

726 The authors have declared that no competing interests exist.

727

728 **Author contributions**

729 NL and MB conducted research, analyzed data, and wrote paper. JMP, SER, AL, MP, GA, and
730 WA conducted research and analyzed data. AK and RKT provided valuable reagents and
731 feedback. SS and JML designed the research and wrote the paper. ENBG designed research,
732 performed experiments, and wrote the paper. JML, SS and ENBG had responsibility for the final
733 content. All authors read and approved the final manuscript.

734

735

736 **Figures and Legends**

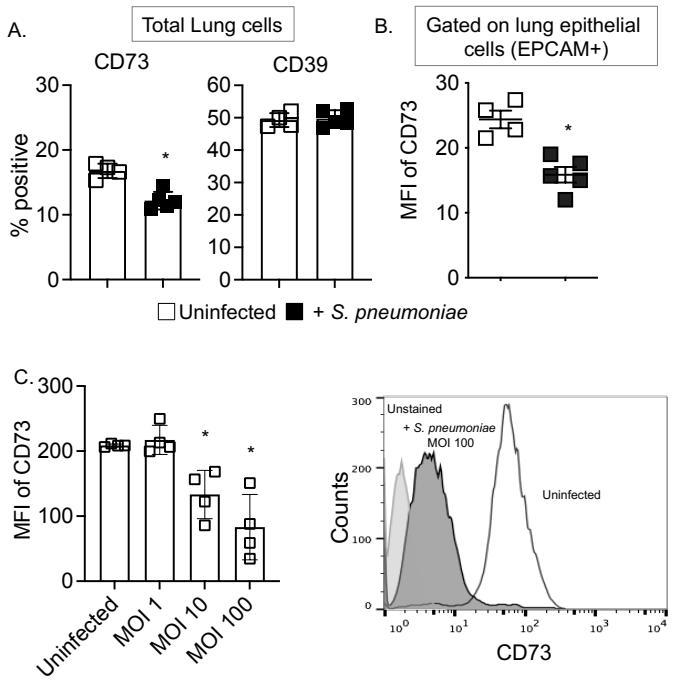

737

738 **Figure 1: Pulmonary infection by *S. pneumoniae* significantly reduces CD73 expression on**
739 **the surface of lung epithelial cells**. C57BL/6 (8-weeks old) male mice were infected intra-
740 tracheally with $2x10^6$ CFU of *S. pneumoniae* TIGR4 strain or mock infected with PBS. Mice were
741 euthanized 48 hpi, the lungs harvested and digested into a single cell suspension, and surface
742 stained for CD73 and CD39. Flow cytometry was used to determine (A) the percentage of $CD73^+$
743 and $CD39^+$ total lung cells and (B) the expression (mean fluorescent intensity or MFI) of CD73 on
744 lung epithelial cells (gated on EPCAM+ cell population). The data shown are pooled from 4-5
745 mice per group with each box representing one mouse. *, $p< 0.05$ by Student's t-test indicate
746 significant differences from uninfected controls. (C) H292 cells were challenged with *S.*
747 *pneumoniae* TIGR4 strain at indicated MOIs for 1 h and MFI of surface exposed CD73 was
748 measured by flow cytometry. The panel on the right shows a representative histogram showing
749 the intensity of CD73 labeling comparing uninfected and infected conditions. Data are pooled from
750 four independent experiments. *, $p< 0.05$ by One-way ANOVA followed by Dunnet's test.

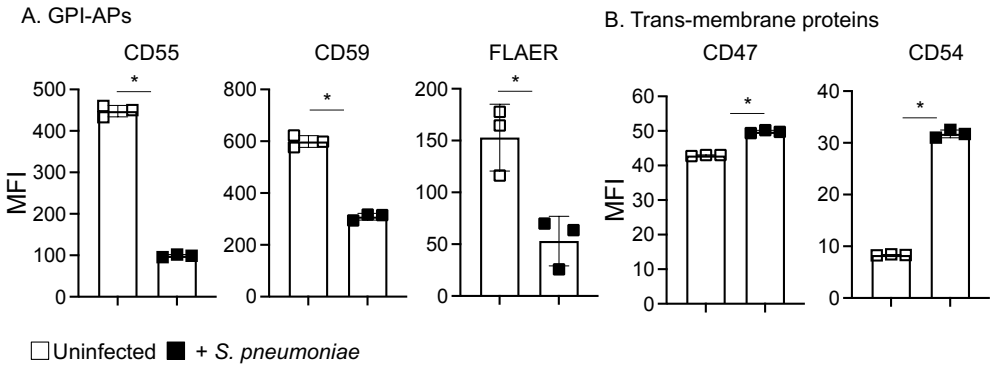

751

752 **Figure 2: *S. pneumoniae* infection of lung epithelial cell lines decreases surface associated**
753 **Glycosylphosphatidylinositol anchored proteins (GPI-APs)**. H292 cells were infected with *S.*
754 *pneumoniae* TIGR4 strain at an MOI of 10 for 1 h. Flow cytometry was used to measure the
755 expression (MFI) of (A) CD55 and CD59, GPI-APs detected using specific antibodies, and of bulk
756 GPI-APs detected by using the fluorescent-labeled mutant of aerolysin (FLAER) or (B) CD47 and
757 CD54, both transmembrane proteins detected by using specific antibodies. Data are pooled from
758 three independent experiments. *, $p < 0.05$ by Student's t-test indicates significant differences from
759 uninfected controls.

760

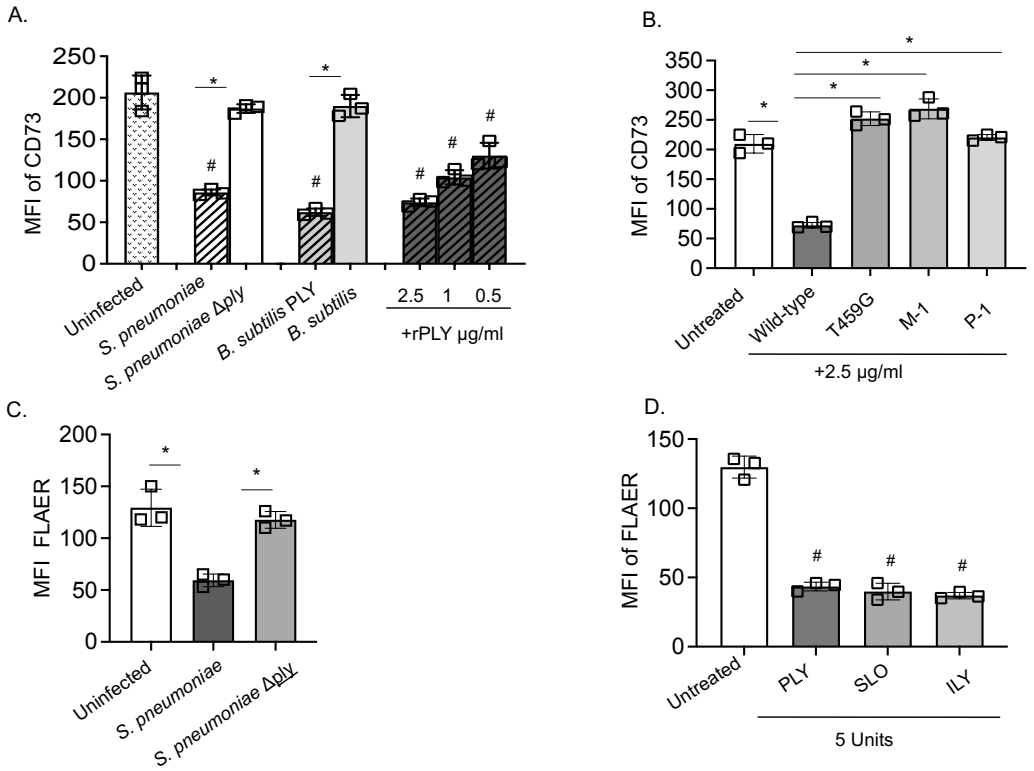

Figure 3: The decrease in cell surface expression of GPI-APs is dependent on PLY and its pore formation capacity. H292 cells were infected with the indicated bacterial strains at an MOI of 10 or treated with the indicated concentrations of recombinant toxins for 1h (A-B) or 10 min (C-D). The cells were then stained and the MFI of CD73 or FLAER was measured by flow cytometry. Data pooled from three independent experiments are shown. #, $p < 0.05$ indicates significant differences from uninfected controls and *, $p < 0.05$ indicates significant differences between the indicated groups by One-way ANOVA followed by Tukey's test (A-C) or Dunnet's test (D). Units for the indicated toxins were determined by their ability to induce pores in the cells. 1U of toxin is equivalent to the concentration of toxin that causes pores in 50% of the cells. rPLY (recombinant PLY), PLY (Pneumolysin), SLO (Streptolysin O) and ILY (intermedilysin). T459G, M-1 and P-1 refer to *S. pneumoniae* strains expressing mutant forms of PLY that cannot form fully functional pores (see Materials & Methods).

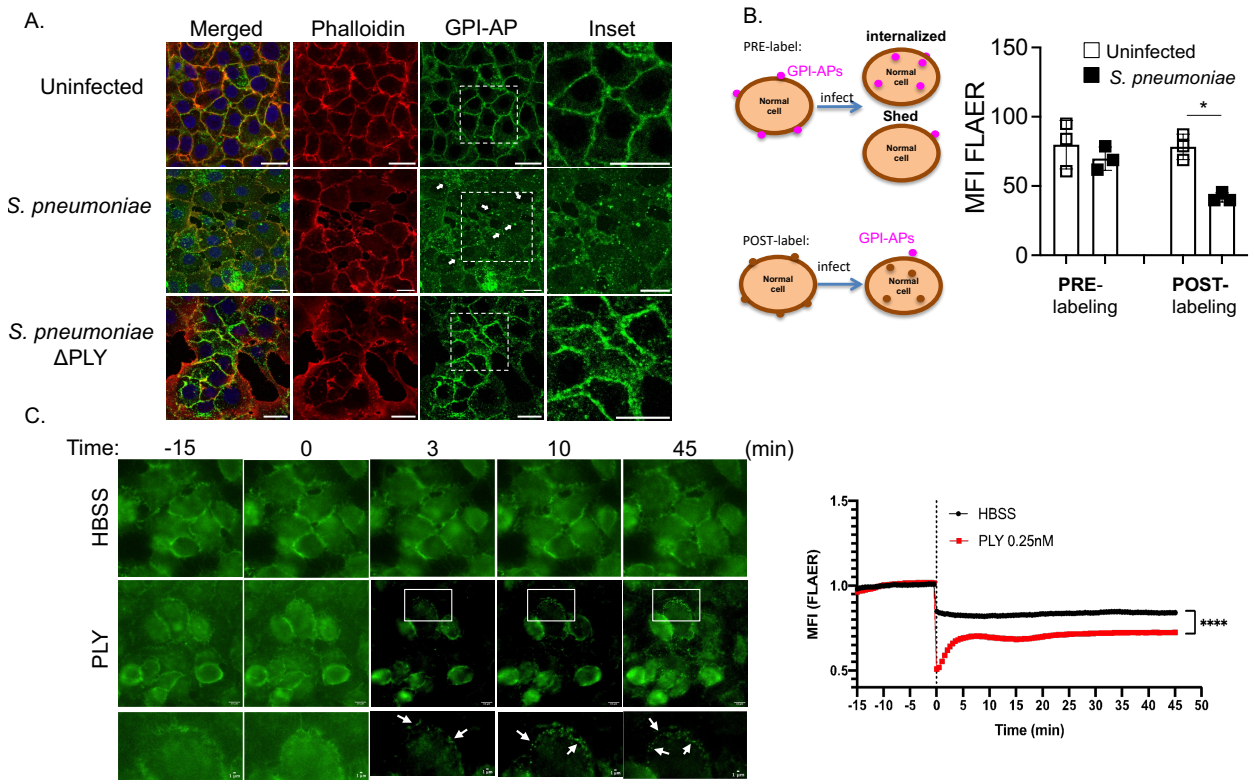

Figure 4: Infection with *S. pneumoniae* triggers the internalization of GPI-APs from the host cell surface. (A) H292 cells were infected with wildtype or *S. pneumoniae* Δ*ply* at an MOI of 20 for 1 h, fixed with PFA for 20 min, permeabilized with 0.1% Tx-100 and stained with phalloidin (to detect actin filaments**,** red) and FLAER (to detect GPI-APS, green). White arrows point GPI-APs concentrating intracellularly into vesicle-like structures. Insets highlight FLAER staining in the different conditions. Bars indicate a 20 µm scale. Representative images from four independent experiments are shown. (B) Left panel shows the schematic illustration of FLAER labeling of H292 cells either pre- or post-infection with *S. pneumoniae* TIGR4 strain (MOI of 10 for 1 h). The right panel shows the MFI of FLAER measured by flow cytometry. Data pooled from three independent experiments are shown. *, $p < 0.05$ indicates significant differences between the indicated groups by One-way ANOVA followed by Tukey's test. (C) The left panel shows sequential frames of time-lapse microscopy video of HeLa cells pre-labeled with FLAER and challenged with PLY (0.25 nM) or HBSS (control). PLY was added at time point 0 min. The inset

789 shows detailed distribution of GPI-APs up to 45 min post PLY challenge. The right panel shows
790 quantified MFI for the FLAER signal overtime. Image analysis was performed using ImageJ by
791 randomly selecting a region of interest (ROI) in the membrane of at least 53 cells per condition
792 and calculating MFI overtime. The values were then normalized to the mean MFI calculated
793 before adding PLY or HBSS. Scale bar for the middle lane is 10 μm and for the bottom lane is 1
794 μm. White arrows in the bottom lane indicate where GPI-APs appear in "vesicle-like" structures
795 likely inside the cells. *, $p<0.05$ by Student's paired t-test.

796

797

798

799

800

801

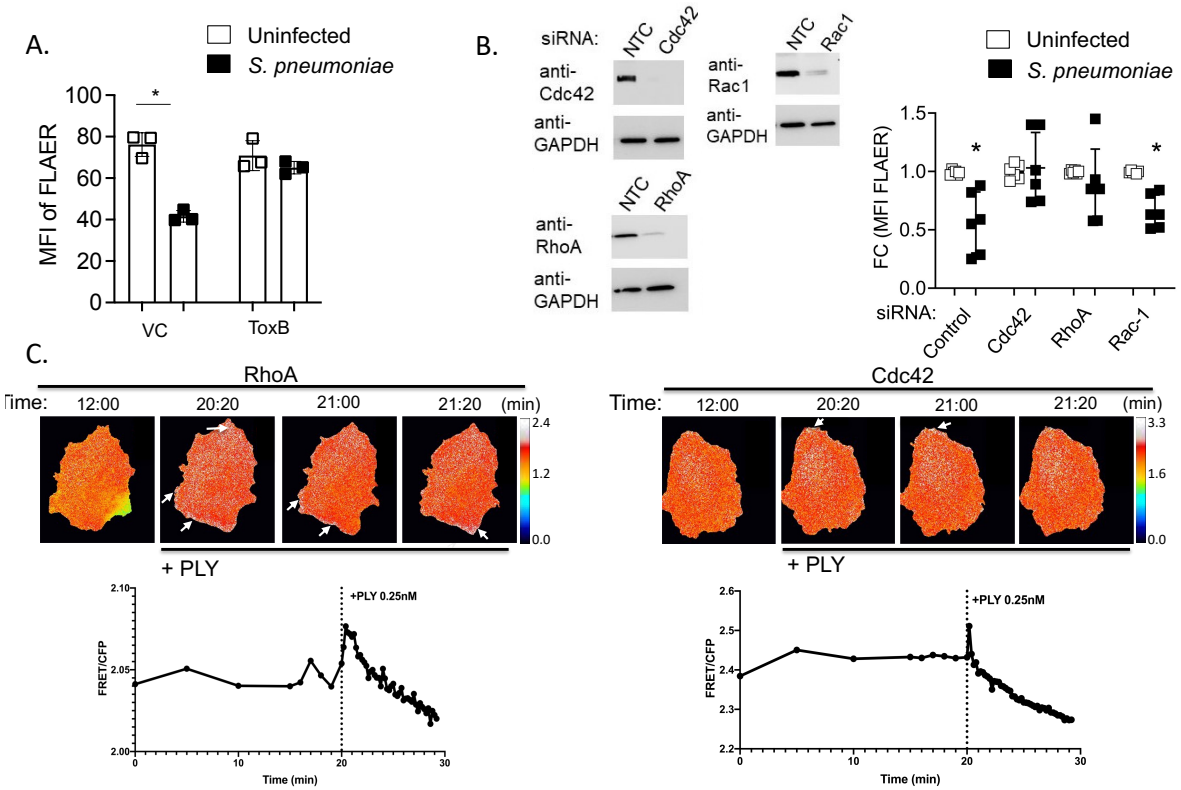

Figure 5: Removal of GPI-APs from the cell surface largely depends on host GTPases RhoA and Cdc42 activity. (A) H292 cells were pre-treated with 100 ng/ml *C. difficile* toxin B (Tox B) or vehicle control (VC) overnight and infected with *S. pneumoniae* TIGR4 strain at an MOI of 10 for 30 min, labeled with FLAER and the MFI was assessed by flow cytometry. Data are pooled from three independent experiments. *, $p < 0.05$ by One-way ANOVA followed by Tukey's test. (B) H292 cells were transfected with a control non-targeting (NTC) siRNA, or siRNA targeting GTPases Cdc42, RhoA and Rac1. At 48 h post-transfection, whole cell lysates were used to confirm the depletion of the target proteins through Western blotting. Detection of GAPDH was used as a loading control (left panel). Depleted and control cells were infected with *S. pneumoniae* TIGR4 at an MOI of 10 for 30 min, labeled with FLAER and the MFI assessed by flow cytometry (right panel). The MFI values of FLAER are displayed as fold changes with respect to the uninfected baseline for the respective siRNA condition. The data shown are the mean of three independent experiments done in duplicates. *, $p < 0.05$ indicates significantly different than 1 by

816 one-sample t-test. (C) HeLa cells over-expressing a FRET probe for RhoA or Cdc42 were imaged
817 for 20 min before and 10 min after incubation with 0.25 nM of PLY. The upper panel shows
818 representative sequential frames of time-lapse images of HeLa cells before and after incubation
819 with PLY. FRET/CFP ratio images are shown in blue-to-white pseudocolor scale with white being
820 high activation. Arrows show the regions where RhoA (left) or Cdc42 (right) are activated
821 (FRET/CFP signal is high). The lower panel shows the quantitative analysis for the ratio between
822 the FRET and CFP signal (FRET/CFP), which measures the RhoA and Cdc42 activation levels.
823 The quantification was performed using a custom-made macro to calculate FRET/CFP ratio
824 specifically at the cell membrane. 79 cells (for RhoA) and 74 cells (for Cdc42) were analyzed from
825 two independent experiments.

826

827

828

829

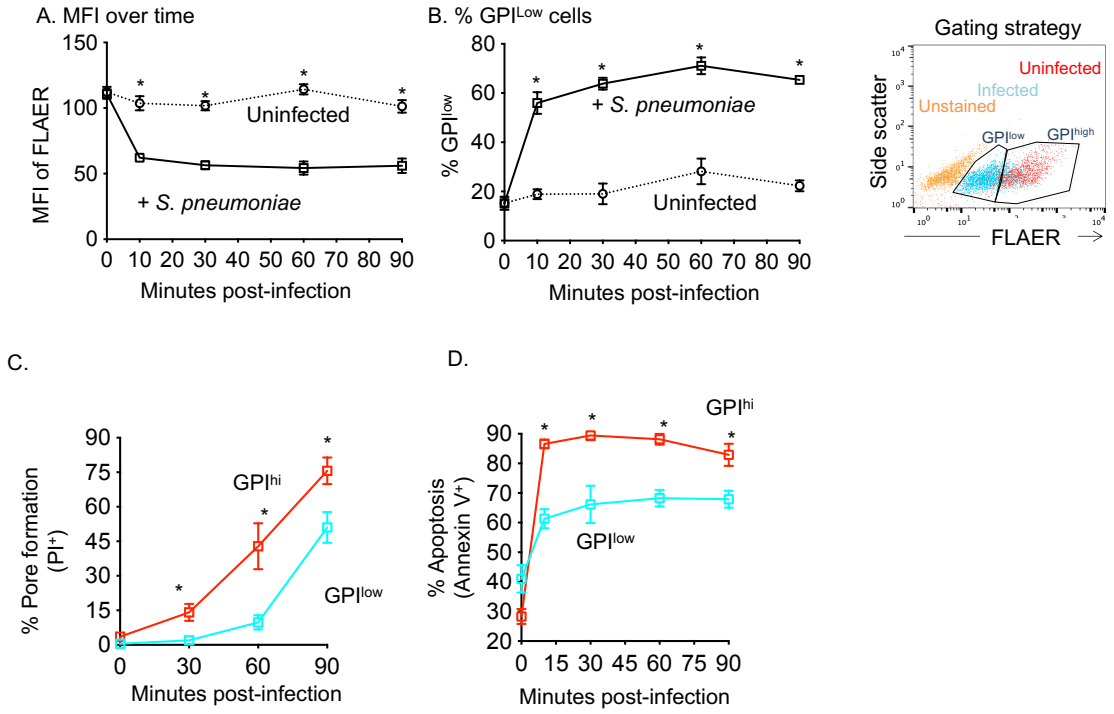

Figure 6: Internalization of GPI-APs is associated with lower levels of PLY-induced cellular damage. H292 cells were infected with *S. pneumoniae* TIGR4 strain at an MOI of 10 or left uninfected. The cells were then labeled with FLAER and flow cytometry was used to measure (A) the MFI of FLAER at indicated time points of infection and (B) calculate the percentage of H292 cells (left panel) with down-regulated FLAER expression (termed as GPI^{low}) based upon the gating strategy shown in the right panel. (C) H292 cells suspended in media containing propidium iodide (PI) were infected with *S. pneumoniae* TIGR4 strain at an MOI of 10 and labeled with FLAER. GPI^{low} vs GPI^{hi} cell populations were then gated on, as indicated in the left panel of (B) and the percentage of H292 cells within each population that incorporated the PI dye was assessed by flow cytometry. (D) H292 cells were infected with *S. pneumoniae* for the indicated times and stained with Annexin V and FLAER. GPI^{low} vs GPI^{hi} populations were gated (right panel in B) and the percentage of apoptotic (Annexin V +) cells within each population was determined through flow cytometry. Data pooled from three independent experiments are shown. * $p < 0.05$ indicate differences by one-way ANOVA comparison between the different groups at indicated time points.

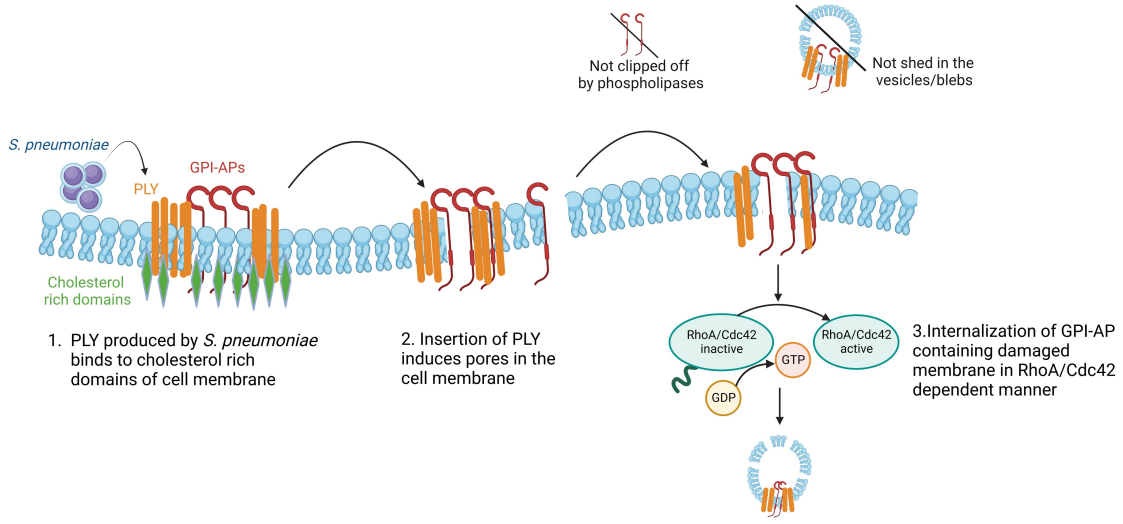

Figure 7: Working Model. PLY inserts in cholesterol-rich microdomains where GPI-APs are colocalized. PLY-induced pores trigger membrane repair resulting in internalization of the GPI-AP containing damaged membrane in a RhoA/Cdc42-dependent manner.

860 **References:**

861 1. Estimates of the global, regional, and national morbidity, mortality, and aetiologies of lower
862 respiratory infections in 195 countries, 1990-2016: a systematic analysis for the Global Burden of
863 Disease Study 2016. Lancet Infect Dis. 2018;18(11):1191-210. Epub 2018/09/24. doi:
864 10.1016/s1473-3099(18)30310-4. PubMed PMID: 30243584; PubMed Central PMCID:
865 PMCPMC6202443.

866 2. Organization WH. Pneumonia in children. . Accessed April 2, 2024. doi:
867 https://www.who.int/news-room/fact-sheets/detail/pneumonia.

868 3. van der Poll T, Opal SM. Pathogenesis, treatment, and prevention of pneumococcal
869 pneumonia. Lancet. 2009;374(9700):1543-56. Epub 2009/11/03. doi: 10.1016/S0140-
870 6736(09)61114-4. PubMed PMID: 19880020.

871 4. Randle E, Ninis N, Inwald D. Invasive pneumococcal disease. Archives of disease in
872 childhood - Education & practice edition. 2011;96(5):183-90. doi: 10.1136/adc.2010.191718.

873 5. Ganaie F, Saad Jamil S, McGee L, van Tonder Andries J, Bentley Stephen D, Lo
874 Stephanie W, et al. A New Pneumococcal Capsule Type, 10D, is the 100th Serotype and Has a
875 Large cps Fragment from an Oral Streptococcus. mBio. 11(3):e00937-20. doi:
876 10.1128/mBio.00937-20.

877 6. Weiser JN, Ferreira DM, Paton JC. Streptococcus pneumoniae: transmission, colonization
878 and invasion. Nat Rev Microbiol. 2018;16(6):355-67. Epub 2018/03/31. doi: 10.1038/s41579-018-
879 0001-8. PubMed PMID: 29599457; PubMed Central PMCID: PMCPMC5949087.

880 7. Obaro S, Adegbola R. The pneumococcus: carriage, disease and conjugate vaccines.
881 Journal of medical microbiology. 2002;51(2):98-104. Epub 2002/02/28. doi: 10.1099/0022-1317-
882 51-2-98. PubMed PMID: 11863272.

883 8. AlonsoDeVelasco E, Verheul AF, Verhoef J, Snippe H. Streptococcus pneumoniae:
884 virulence factors, pathogenesis, and vaccines. Microbiol Rev. 1995;59(4):591-603. Epub

885 1995/12/01. doi: 10.1128/mr.59.4.591-603.1995. PubMed PMID: 8531887; PubMed Central
886 PMCID: PMCPMC239389.
887 9. Rubins JB, Charboneau D, Fasching C, Berry AM, Paton JC, Alexander JE, et al. Distinct
888 roles for pneumolysin's cytotoxic and complement activities in the pathogenesis of pneumococcal
889 pneumonia. Am J Respir Crit Care Med. 1996;153(4 Pt 1):1339-46. Epub 1996/04/01. doi:
890 10.1164/ajrccm.153.4.8616564. PubMed PMID: 8616564.
891 10. Mitchell TJ, Andrew PW, Saunders FK, Smith AN, Boulnois GJ. Complement activation
892 and antibody binding by pneumolysin via a region of the toxin homologous to a human acute-
893 phase protein. Mol Microbiol. 1991;5(8):1883-8. Epub 1991/08/01. doi: 10.1111/j.1365-
894 2958.1991.tb00812.x. PubMed PMID: 1766369.
895 11. Adams W, Bhowmick R, Bou Ghanem EN, Wade K, Shchepetov M, Weiser JN, et al.
896 Pneumolysin Induces 12-Lipoxygenase–Dependent Neutrophil Migration during
897 Streptococcus pneumoniae Infection. The Journal of Immunology. 2020;204(1):101-
898 11. doi: 10.4049/jimmunol.1800748.
899 12. Nishimoto AT, Rosch JW, Tuomanen EI. Pneumolysin: Pathogenesis and Therapeutic
900 Target. Frontiers in Microbiology. 2020;11. doi: 10.3389/fmicb.2020.01543.
901 13. Pereira JM, Xu S, Leong JM, Sousa S. The Yin and Yang of Pneumolysin During
902 Pneumococcal Infection. Frontiers in Immunology. 2022;13. doi: 10.3389/fimmu.2022.878244.
903 14. Tweten RK, Hotze EM, Wade KR. The Unique Molecular Choreography of Giant Pore
904 Formation by the Cholesterol-Dependent Cytolysins of Gram-Positive Bacteria. Annu Rev
905 Microbiol. 2015;69:323-40. Epub 2015/10/22. doi: 10.1146/annurev-micro-091014-104233.
906 PubMed PMID: 26488276; PubMed Central PMCID: PMCPMC7875328.
907 15. Shatursky O, Heuck AP, Shepard LA, Rossjohn J, Parker MW, Johnson AE, et al. The
908 mechanism of membrane insertion for a cholesterol-dependent cytolysin: a novel paradigm for
909 pore-forming toxins. Cell. 1999;99(3):293-9. Epub 1999/11/11. doi: 10.1016/s0092-
910 8674(00)81660-8. PubMed PMID: 10555145.

911 16. Dang TX, Hotze EM, Rouiller I, Tweten RK, Wilson-Kubalek EM. Prepore to pore transition
912 of a cholesterol-dependent cytolysin visualized by electron microscopy. J Struct Biol.
913 2005;150(1):100-8. Epub 2005/03/31. doi: 10.1016/j.jsb.2005.02.003. PubMed PMID: 15797734.
914 17. van Pee K, Neuhaus A, D'Imprima E, Mills DJ, Kühlbrandt W, Yildiz Ö. CryoEM structures
915 of membrane pore and prepore complex reveal cytolytic mechanism of Pneumolysin. eLife.
916 2017;6:e23644. doi: 10.7554/eLife.23644.
917 18. Berry AM, Yother J, Briles DE, Hansman D, Paton JC. Reduced virulence of a defined
918 pneumolysin-negative mutant of Streptococcus pneumoniae. Infect Immun. 1989;57(7):2037-42.
919 Epub 1989/07/01. doi: 10.1128/iai.57.7.2037-2042.1989. PubMed PMID: 2731982; PubMed
920 Central PMCID: PMCPMC313838.
921 19. Diep DB, Nelson KL, Raja SM, Pleshak EN, Buckley JT. Glycosylphosphatidylinositol
922 anchors of membrane glycoproteins are binding determinants for the channel-forming toxin
923 aerolysin. J Biol Chem. 1998;273(4):2355-60. Epub 1998/01/27. doi: 10.1074/jbc.273.4.2355.
924 PubMed PMID: 9442081.
925 20. Fujihara Y, Ikawa M. GPI-AP release in cellular, developmental, and reproductive biology.
926 J Lipid Res. 2016;57(4):538-45. Epub 2015/11/26. doi: 10.1194/jlr.R063032. PubMed PMID:
927 26593072; PubMed Central PMCID: PMCPMC4808780.
928 21. Ikezawa H. Glycosylphosphatidylinositol (GPI)-anchored proteins. Biol Pharm Bull.
929 2002;25(4):409-17. Epub 2002/05/09. doi: 10.1248/bpb.25.409. PubMed PMID: 11995915.
930 22. Zurzolo C, Simons K. Glycosylphosphatidylinositol-anchored proteins: Membrane
931 organization and transport. Biochimica et Biophysica Acta (BBA) - Biomembranes.
932 2016;1858(4):632-9. doi: https://doi.org/10.1016/j.bbamem.2015.12.018.
933 23. Lopez S, Rodriguez-Gallardo S, Sabido-Bozo S, Muñiz M. Endoplasmic Reticulum Export
934 of GPI-Anchored Proteins. International Journal of Molecular Sciences. 2019;20(14):3506.
935 PubMed PMID: doi:10.3390/ijms20143506.

936 24. Kinoshita T. Biosynthesis and biology of mammalian GPI-anchored proteins. Open
937 Biology. 2020;10(3):190290. doi: doi:10.1098/rsob.190290.
938 25. Muñiz M, Zurzolo C. Sorting of GPI-anchored proteins from yeast to mammals--common
939 pathways at different sites? J Cell Sci. 2014;127(Pt 13):2793-801. Epub 2014/06/08. doi:
940 10.1242/jcs.148056. PubMed PMID: 24906797.
941 26. Paladino S, Lebreton S, Tivodar S, Campana V, Tempre R, Zurzolo C. Different GPI-
942 attachment signals affect the oligomerisation of GPI-anchored proteins and their apical sorting. J
943 Cell Sci. 2008;121(Pt 24):4001-7. Epub 2008/12/06. doi: 10.1242/jcs.036038. PubMed PMID:
944 19056670.
945 27. Raghupathy R, Anilkumar AA, Polley A, Singh PP, Yadav M, Johnson C, et al.
946 Transbilayer lipid interactions mediate nanoclustering of lipid-anchored proteins. Cell.
947 2015;161(3):581-94. Epub 2015/04/25. doi: 10.1016/j.cell.2015.03.048. PubMed PMID:
948 25910209; PubMed Central PMCID: PMCPMC4651428.
949 28. Lebreton S, Zurzolo C, Paladino S. Organization of GPI-anchored proteins at the cell
950 surface and its physiopathological relevance. Crit Rev Biochem Mol Biol. 2018;53(4):403-19.
951 Epub 2018/07/25. doi: 10.1080/10409238.2018.1485627. PubMed PMID: 30040489.
952 29. Sabharanjak S, Sharma P, Parton RG, Mayor S. GPI-Anchored Proteins Are Delivered to
953 Recycling Endosomes via a Distinct cdc42-Regulated, Clathrin-Independent Pinocytic Pathway.
954 Developmental Cell. 2002;2(4):411-23. doi: https://doi.org/10.1016/S1534-5807(02)00145-4.
955 30. Hodge RG, Ridley AJ. Regulating Rho GTPases and their regulators. Nat Rev Mol Cell
956 Biol. 2016;17(8):496-510. Epub 2016/06/16. doi: 10.1038/nrm.2016.67. PubMed PMID:
957 27301673.
958 31. Heasman SJ, Ridley AJ. Mammalian Rho GTPases: new insights into their functions from
959 in vivo studies. Nat Rev Mol Cell Biol. 2008;9(9):690-701. Epub 2008/08/23. doi:
960 10.1038/nrm2476. PubMed PMID: 18719708.

961 32. Chadda R, Howes MT, Plowman SJ, Hancock JF, Parton RG, Mayor S. Cholesterol-
962 sensitive Cdc42 activation regulates actin polymerization for endocytosis via the GEEC pathway.
963 Traffic. 2007;8(6):702-17. Epub 2007/04/28. doi: 10.1111/j.1600-0854.2007.00565.x. PubMed
964 PMID: 17461795.
965 33. Hasko G, Linden J, Cronstein B, Pacher P. Adenosine receptors: therapeutic aspects for
966 inflammatory and immune diseases. Nature reviews Drug discovery. 2008;7(9):759-70. Epub
967 2008/09/02. doi: 10.1038/nrd2638. PubMed PMID: 18758473; PubMed Central PMCID:
968 PMC2568887.
969 34. Bou Ghanem EN, Clark S, Roggensack SE, McIver SR, Alcaide P, Haydon PG, et al.
970 Extracellular Adenosine Protects against Streptococcus pneumoniae Lung Infection by
971 Regulating Pulmonary Neutrophil Recruitment. PLoS pathogens. 2015;11(8):e1005126. Epub
972 2015/08/28. doi: 10.1371/journal.ppat.1005126. PubMed PMID: 26313746; PubMed Central
973 PMCID: PMC4552087.
974 35. Siwapornchai N, Lee JN, Tchalla EYI, Bhalla M, Yeoh JH, Roggensack SE, et al.
975 Extracellular adenosine enhances the ability of PMNs to kill Streptococcus pneumoniae by
976 inhibiting IL-10 production. J Leukoc Biol. 2020. Epub 2020/02/06. doi: 10.1002/JLB.4MA0120-
977 115RR. PubMed PMID: 32017200.
978 36. Bhalla M, Heinzinger LR, Morenikeji OB, Marzullo B, Thomas BN, Bou Ghanem EN.
979 Transcriptome profiling reveals CD73 and age-driven changes in neutrophil responses against
980 Streptococcus pneumoniae. Infect Immun. 2021:Iai0025821. Epub 2021/07/27. doi:
981 10.1128/iai.00258-21. PubMed PMID: 34310891.
982 37. Bhalla M, Simmons SR, Abamonte A, Herring SE, Roggensack SE, Bou Ghanem EN.
983 Extracellular adenosine signaling reverses the age-driven decline in the ability of neutrophils to
984 kill Streptococcus pneumoniae. Aging Cell. 2020:e13218. Epub 2020/08/14. doi:
985 10.1111/acel.13218. PubMed PMID: 32790148.

986 38. Bhalla M, Hui Yeoh J, Lamneck C, Herring SE, Tchalla EYI, Heinzinger LR, et al. A1
987 adenosine receptor signaling reduces Streptococcus pneumoniae adherence to pulmonary
988 epithelial cells by targeting expression of platelet-activating factor receptor. Cellular microbiology.
989 2020;22(2):e13141. Epub 2019/11/12. doi: 10.1111/cmi.13141. PubMed PMID: 31709673.
990 39. Bhowmick R, Tin Maung NH, Hurley BP, Ghanem EB, Gronert K, McCormick BA, et al.
991 Systemic disease during Streptococcus pneumoniae acute lung infection requires 12-
992 lipoxygenase-dependent inflammation. J Immunol. 2013;191(10):5115-23. Epub 2013/10/04. doi:
993 10.4049/jimmunol.1300522. PubMed PMID: 24089193; PubMed Central PMCID: PMC3836588.
994 40. Yonker LM, Pazos MA, Lanter BB, Mou H, Chu KK, Eaton AD, et al. Neutrophil-Derived
995 Cytosolic PLA2alpha Contributes to Bacterial-Induced Neutrophil Transepithelial Migration. J
996 Immunol. 2017;199(8):2873-84. Epub 2017/09/10. doi: 10.4049/jimmunol.1700539. PubMed
997 PMID: 28887431; PubMed Central PMCID: PMC5636676.
998 41. Choi CH, Lee JS, Lee YC, Park TI, Lee JC. Acinetobacter baumannii invades epithelial
999 cells and outer membrane protein A mediates interactions with epithelial cells. BMC microbiology.
1000 2008;8:216. Epub 2008/12/11. doi: 10.1186/1471-2180-8-216. PubMed PMID: 19068136;
1001 PubMed Central PMCID: PMC2615016.
1002 42. Antonioli L, Pacher P, Vizi ES, Haskó G. CD39 and CD73 in immunity and inflammation.
1003 Trends Mol Med. 2013;19(6):355-67. Epub 2013/04/23. doi: 10.1016/j.molmed.2013.03.005.
1004 PubMed PMID: 23601906; PubMed Central PMCID: PMCPMC3674206.
1005 43. Brodsky RA, Mukhina GL, Li S, Nelson KL, Chiurazzi PL, Buckley JT, et al. Improved
1006 detection and characterization of paroxysmal nocturnal hemoglobinuria using fluorescent
1007 aerolysin. Am J Clin Pathol. 2000;114(3):459-66. Epub 2000/09/16. doi: 10.1093/ajcp/114.3.459.
1008 PubMed PMID: 10989647; PubMed Central PMCID: PMCPMC4124633.
1009 44. Paladino S, Lebreton S, Lelek M, Riccio P, De Nicola S, Zimmer C, et al. GPI-anchored
1010 proteins are confined in subdiffraction clusters at the apical surface of polarized epithelial cells.

1011 Biochem J. 2017;474(24):4075-90. Epub 2017/10/20. doi: 10.1042/bcj20170582. PubMed PMID:
1012 29046391; PubMed Central PMCID: PMCPMC5712066.
1013 45. Au - Kusek ME, Au - Pazos MA, Au - Pirzai W, Au - Hurley BP. In vitro Coculture Assay
1014 to Assess Pathogen Induced Neutrophil Trans-epithelial Migration. JoVE. 2014;(83):e50823. doi:
1015 doi:10.3791/50823.
1016 46. Farrand AJ, LaChapelle S, Hotze EM, Johnson AE, Tweten RK. Only two amino acids are
1017 essential for cytolytic toxin recognition of cholesterol at the membrane surface. Proceedings of
1018 the National Academy of Sciences. 2010;107(9):4341-6. doi: doi:10.1073/pnas.0911581107.
1019 47. Shepard LA, Heuck AP, Hamman BD, Rossjohn J, Parker MW, Ryan KR, et al.
1020 Identification of a membrane-spanning domain of the thiol-activated pore-forming toxin
1021 Clostridium perfringens perfringolysin O: an alpha-helical to beta-sheet transition identified by
1022 fluorescence spectroscopy. Biochemistry. 1998;37(41):14563-74. Epub 1998/10/17. doi:
1023 10.1021/bi981452f. PubMed PMID: 9772185.
1024 48. Schmeck B, Gross R, N'Guessan PD, Hocke AC, Hammerschmidt S, Mitchell TJ, et al.
1025 Streptococcus pneumoniae-induced caspase 6-dependent apoptosis in lung epithelium. Infect
1026 Immun. 2004;72(9):4940-7. Epub 2004/08/24. doi: 10.1128/iai.72.9.4940-4947.2004. PubMed
1027 PMID: 15321985; PubMed Central PMCID: PMCPMC517413.
1028 49. Marriott HM, Mitchell TJ, Dockrell DH. Pneumolysin: a double-edged sword during the
1029 host-pathogen interaction. Curr Mol Med. 2008;8(6):497-509. Epub 2008/09/11. doi:
1030 10.2174/156652408785747924. PubMed PMID: 18781957.
1031 50. Heuck AP, Moe PC, Johnson BB. The cholesterol-dependent cytolysin family of gram-
1032 positive bacterial toxins. Subcell Biochem. 2010;51:551-77. Epub 2010/03/10. doi: 10.1007/978-
1033 90-481-8622-8_20. PubMed PMID: 20213558.
1034 51. Paulick MG, Bertozzi CR. The Glycosylphosphatidylinositol Anchor: A Complex
1035 Membrane-Anchoring Structure for Proteins. Biochemistry. 2008;47(27):6991-7000. doi:
1036 10.1021/bi8006324.

1037 52. Asmat TM, Agarwal V, Räth S, Hildebrandt JP, Hammerschmidt S. Streptococcus
1038 pneumoniae infection of host epithelial cells via polymeric immunoglobulin receptor transiently
1039 induces calcium release from intracellular stores. J Biol Chem. 2011;286(20):17861-9. Epub
1040 2011/04/02. doi: 10.1074/jbc.M110.212225. PubMed PMID: 21454571; PubMed Central PMCID:
1041 PMCPMC3093861.
1042 53. Takenouchi T, Ogihara K, Sato M, Kitani H. Inhibitory effects of U73122 and U73343 on
1043 Ca2+ influx and pore formation induced by the activation of P2X7 nucleotide receptors in mouse
1044 microglial cell line. Biochim Biophys Acta. 2005;1726(2):177-86. Epub 2005/08/27. doi:
1045 10.1016/j.bbagen.2005.08.001. PubMed PMID: 16122875.
1046 54. Letsiou E, Teixeira Alves LG, Fatykhova D, Felten M, Mitchell TJ, Müller-Redetzky HC, et
1047 al. Microvesicles released from pneumolysin-stimulated lung epithelial cells carry mitochondrial
1048 cargo and suppress neutrophil oxidative burst. Scientific Reports. 2021;11(1):9529. doi:
1049 10.1038/s41598-021-88897-y.
1050 55. Alves S, Pereira JM, Mayer RL, Gonçalves ADA, Impens F, Cabanes D, et al. Cells
1051 Responding to Closely Related Cholesterol-Dependent Cytolysins Release Extracellular Vesicles
1052 with a Common Proteomic Content Including Membrane Repair Proteins. Toxins (Basel).
1053 2022;15(1). Epub 2023/01/21. doi: 10.3390/toxins15010004. PubMed PMID: 36668824; PubMed
1054 Central PMCID: PMCPMC9865450.
1055 56. Babiychuk EB, Monastyrskaya K, Potez S, Draeger A. Blebbing confers resistance against
1056 cell lysis. Cell Death Differ. 2011;18(1):80-9. Epub 2010/07/03. doi: 10.1038/cdd.2010.81.
1057 PubMed PMID: 20596076; PubMed Central PMCID: PMCPMC3131879.
1058 57. Wolfmeier H, Radecke J, Schoenauer R, Koeffel R, Babiychuk VS, Drücker P, et al. Active
1059 release of pneumolysin prepores and pores by mammalian cells undergoing a Streptococcus
1060 pneumoniae attack. Biochim Biophys Acta. 2016;1860(11 Pt A):2498-509. Epub 2016/08/03. doi:
1061 10.1016/j.bbagen.2016.07.022. PubMed PMID: 27481675.

1062 58. Limouze J, Straight AF, Mitchison T, Sellers JR. Specificity of blebbistatin, an inhibitor of
1063 myosin II. J Muscle Res Cell Motil. 2004;25(4-5):337-41. Epub 2004/11/19. doi: 10.1007/s10974-
1064 004-6060-7. PubMed PMID: 15548862.
1065 59. Yarar D, Waterman-Storer CM, Schmid SL. A Dynamic Actin Cytoskeleton Functions at
1066 Multiple Stages of Clathrin-mediated Endocytosis. Molecular Biology of the Cell. 2005;16(2):964-
1067 75. doi: 10.1091/mbc.e04-09-0774. PubMed PMID: 15601897.
1068 60. Pistor S, Chakraborty T, Niebuhr K, Domann E, Wehland J. The ActA protein of Listeria
1069 monocytogenes acts as a nucleator inducing reorganization of the actin cytoskeleton. Embo j.
1070 1994;13(4):758-63. Epub 1994/02/15. doi: 10.1002/j.1460-2075.1994.tb06318.x. PubMed PMID:
1071 8112291; PubMed Central PMCID: PMCPMC394872.
1072 61. Mayorga LS, Diaz R, Stahl PD. Regulatory role for GTP-binding proteins in endocytosis.
1073 Science. 1989;244(4911):1475-7. Epub 1989/06/23. doi: 10.1126/science.2499930. PubMed
1074 PMID: 2499930.
1075 62. Aktories K, Schmidt G, Just I. Rho GTPases as Targets of Bacterial Protein Toxins.
1076 2000;381(5-6):421-6. doi: doi:10.1515/BC.2000.054.
1077 63. Iliev AI, Djannatian JR, Nau R, Mitchell TJ, Wouters FS. Cholesterol-dependent actin
1078 remodeling via RhoA and Rac1 activation by the Streptococcus pneumoniae toxin
1079 pneumolysin. Proceedings of the National Academy of Sciences. 2007;104(8):2897-902. doi:
1080 doi:10.1073/pnas.0608213104.
1081 64. Tweten RK. Cholesterol-dependent cytolysins, a family of versatile pore-forming toxins.
1082 Infect Immun. 2005;73(10):6199-209. Epub 2005/09/24. doi: 10.1128/iai.73.10.6199-6209.2005.
1083 PubMed PMID: 16177291; PubMed Central PMCID: PMCPMC1230961.
1084 65. Brito C, Cabanes D, Sarmento Mesquita F, Sousa S. Mechanisms protecting host cells
1085 against bacterial pore-forming toxins. Cell Mol Life Sci. 2019;76(7):1319-39. Epub 2018/12/29.
1086 doi: 10.1007/s00018-018-2992-8. PubMed PMID: 30591958; PubMed Central PMCID:
1087 PMCPMC6420883.

1088 66. Casadevall A, Pirofski La. Host-Pathogen Interactions: The Attributes of Virulence. The
1089 Journal of Infectious Diseases. 2001;184(3):337-44. doi: 10.1086/322044.
1090 67. Casadevall A, Pirofski LA. Host-pathogen interactions: basic concepts of microbial
1091 commensalism, colonization, infection, and disease. Infect Immun. 2000;68(12):6511-8. Epub
1092 2000/11/18. doi: 10.1128/iai.68.12.6511-6518.2000. PubMed PMID: 11083759; PubMed Central
1093 PMCID: PMCPMC97744.
1094 68. Brown AO, Millett ER, Quint JK, Orihuela CJ. Cardiotoxicity during invasive pneumococcal
1095 disease. Am J Respir Crit Care Med. 2015;191(7):739-45. Epub 2015/01/30. doi:
1096 10.1164/rccm.201411-1951PP. PubMed PMID: 25629643; PubMed Central PMCID:
1097 PMCPMC4407487.
1098 69. Adams W, Bhowmick R, Bou Ghanem EN, Wade K, Shchepetov M, Weiser JN, et al.
1099 Pneumolysin Induces 12-Lipoxygenase–Dependent Neutrophil Migration during Streptococcus
1100 pneumoniae Infection. The Journal of Immunology. 2020;204(1):101-11. doi:
1101 10.4049/jimmunol.1800748.
1102 70. Reyes LF, Restrepo MI, Hinojosa CA, Soni NJ, Anzueto A, Babu BL, et al. Severe
1103 Pneumococcal Pneumonia Causes Acute Cardiac Toxicity and Subsequent Cardiac Remodeling.
1104 Am J Respir Crit Care Med. 2017;196(5):609-20. Epub 2017/06/15. doi: 10.1164/rccm.201701-
1105 0104OC. PubMed PMID: 28614669; PubMed Central PMCID: PMCPMC5620668.
1106 71. Kadioglu A, Weiser JN, Paton JC, Andrew PW. The role of Streptococcus pneumoniae
1107 virulence factors in host respiratory colonization and disease. Nature reviews Microbiology.
1108 2008;6(4):288-301. Epub 2008/03/15. doi: 10.1038/nrmicro1871. PubMed PMID: 18340341.
1109 72. Price KE, Camilli A. Pneumolysin localizes to the cell wall of Streptococcus pneumoniae.
1110 J Bacteriol. 2009;191(7):2163-8. Epub 2009/01/27. doi: 10.1128/jb.01489-08. PubMed PMID:
1111 19168620; PubMed Central PMCID: PMCPMC2655535.

1112 73. Martins R, Carlos AR, Braza F, Thompson JA, Bastos-Amador P, Ramos S, et al. Disease
1113 Tolerance as an Inherent Component of Immunity. Annual Review of Immunology.
1114 2019;37(1):405-37. doi: 10.1146/annurev-immunol-042718-041739. PubMed PMID: 30673535.
1115 74. Varma R, Mayor S. GPI-anchored proteins are organized in submicron domains at the cell
1116 surface. Nature. 1998;394(6695):798-801. Epub 1998/09/02. doi: 10.1038/29563. PubMed PMID:
1117 9723621.
1118 75. Shepard LA, Shatursky O, Johnson AE, Tweten RK. The mechanism of pore assembly
1119 for a cholesterol-dependent cytolysin: formation of a large prepore complex precedes the insertion
1120 of the transmembrane beta-hairpins. Biochemistry. 2000;39(33):10284-93. Epub 2000/08/24. doi:
1121 10.1021/bi000436r. PubMed PMID: 10956018.
1122 76. Corrotte M, Fernandes MC, Tam C, Andrews NW. Toxin pores endocytosed during
1123 plasma membrane repair traffic into the lumen of MVBs for degradation. Traffic. 2012;13(3):483-
1124 94. Epub 2012/01/04. doi: 10.1111/j.1600-0854.2011.01323.x. PubMed PMID: 22212686;
1125 PubMed Central PMCID: PMCPMC3356596.
1126 77. Bouillot S, Reboud E, Huber P. Functional Consequences of Calcium Influx Promoted by
1127 Bacterial Pore-Forming Toxins. Toxins (Basel). 2018;10(10). Epub 2018/09/28. doi:
1128 10.3390/toxins10100387. PubMed PMID: 30257425; PubMed Central PMCID:
1129 PMCPMC6215193.
1130 78. Ray S, Roth R, Keyel PA. Membrane repair triggered by cholesterol-dependent cytolysins
1131 is activated by mixed lineage kinases and MEK. Science advances. 2022;8(11):eabl6367. Epub
1132 2022/03/17. doi: 10.1126/sciadv.abl6367. PubMed PMID: 35294243; PubMed Central PMCID:
1133 PMCPMC8926344.
1134 79. Hervé JC, Bourmeyster N. Rho GTPases at the crossroad of signaling networks in
1135 mammals. Small GTPases. 2015;6(2):43-8. Epub 2015/06/26. doi:
1136 10.1080/21541248.2015.1044811. PubMed PMID: 26110743; PubMed Central PMCID:
1137 PMCPMC4601364.

1138 80. Lakhan SE, Sabharanjak S, De A. Endocytosis of glycosylphosphatidylinositol-anchored
1139 proteins. Journal of Biomedical Science. 2009;16(1):93. doi: 10.1186/1423-0127-16-93.
1140 81. Aït-Slimane T, Galmes R, Trugnan G, Maurice M. Basolateral internalization of GPI-
1141 anchored proteins occurs via a clathrin-independent flotillin-dependent pathway in polarized
1142 hepatic cells. Mol Biol Cell. 2009;20(17):3792-800. Epub 2009/07/17. doi: 10.1091/mbc.e09-04-
1143 0275. PubMed PMID: 19605558; PubMed Central PMCID: PMCPMC2735478.
1144 82. Naslavsky N, Weigert R, Donaldson JG. Characterization of a nonclathrin endocytic
1145 pathway: membrane cargo and lipid requirements. Mol Biol Cell. 2004;15(8):3542-52. Epub
1146 2004/05/18. doi: 10.1091/mbc.e04-02-0151. PubMed PMID: 15146059; PubMed Central PMCID:
1147 PMCPMC491817.
1148 83. Fujimoto LM, Roth R, Heuser JE, Schmid SL. Actin Assembly Plays a Variable, but not
1149 Obligatory Role in Receptor-Mediated Endocytosis. Traffic. 2000;1(2):161-71. doi:
1150 https://doi.org/10.1034/j.1600-0854.2000.010208.x.
1151 84. Yao L-H, Rao Y, Bang C, Kurilova S, Varga K, Wang C-Y, et al. Actin Polymerization Does
1152 Not Provide Direct Mechanical Forces for Vesicle Fission during Clathrin-Mediated Endocytosis.
1153 The Journal of Neuroscience. 2013;33(40):15793-8. doi: 10.1523/jneurosci.2171-13.2013.
1154 85. Hyman T, Shmuel M, Altschuler Y. Actin is required for endocytosis at the apical surface
1155 of Madin-Darby canine kidney cells where ARF6 and clathrin regulate the actin cytoskeleton. Mol
1156 Biol Cell. 2006;17(1):427-37. Epub 2005/10/28. doi: 10.1091/mbc.e05-05-0420. PubMed PMID:
1157 16251360; PubMed Central PMCID: PMCPMC1345679.
1158 86. Hänisch J, Kölm R, Wozniczka M, Bumann D, Rottner K, Stradal TE. Activation of a
1159 RhoA/myosin II-dependent but Arp2/3 complex-independent pathway facilitates Salmonella
1160 invasion. Cell Host Microbe. 2011;9(4):273-85. Epub 2011/04/20. doi:
1161 10.1016/j.chom.2011.03.009. PubMed PMID: 21501827.

1162 87. Van Ngo H, Bhalla M, Chen D-Y, Ireton K. A role for host cell exocytosis in InlB-mediated
1163 internalisation of Listeria monocytogenes. Cellular Microbiology. 2017;19(11):e12768. doi:
1164 https://doi.org/10.1111/cmi.12768.
1165 88. Alves S, Pereira JM, Mayer RL, Gonçalves ADA, Impens F, Cabanes D, et al. Cells
1166 Responding to Closely Related Cholesterol-Dependent Cytolysins Release Extracellular Vesicles
1167 with a Common Proteomic Content Including Membrane Repair Proteins. Toxins. 2023;15(1):4.
1168 PubMed PMID: doi:10.3390/toxins15010004.
1169 89. Schmiel DH, Miller VL. Bacterial phospholipases and pathogenesis. Microbes and
1170 Infection. 1999;1(13):1103-12. doi: https://doi.org/10.1016/S1286-4579(99)00205-1.
1171 90. Shichinohe N, Kobayashi D, Izumi A, Hatanaka K, Fujita R, Kinoshita T, et al. Sequential
1172 hydrolysis of FAD by ecto-5′ nucleotidase CD73 and alkaline phosphatase is required
1173 for uptake of vitamin B₂ into cells. Journal of Biological Chemistry. 2022;298(12).
1174 doi: 10.1016/j.jbc.2022.102640.
1175 91. Hasko G, Csoka B, Koscso B, Chandra R, Pacher P, Thompson LF, et al. Ecto-5'-
1176 nucleotidase (CD73) decreases mortality and organ injury in sepsis. J Immunol.
1177 2011;187(8):4256-67. Epub 2011/09/16. doi: 10.4049/jimmunol.1003379. PubMed PMID:
1178 21918191; PubMed Central PMCID: PMC3387540.
1179 92. Tanaka K, Choi J, Cao Y, Stacey G. Extracellular ATP acts as a damage-associated
1180 molecular pattern (DAMP) signal in plants. Frontiers in Plant Science. 2014;5. doi:
1181 10.3389/fpls.2014.00446.
1182 93. Regateiro FS, Cobbold SP, Waldmann H. CD73 and adenosine generation in the creation
1183 of regulatory microenvironments. Clinical and experimental immunology. 2013;171(1):1-7. Epub
1184 2012/12/04. doi: 10.1111/j.1365-2249.2012.04623.x. PubMed PMID: 23199317; PubMed Central
1185 PMCID: PMC3530089.
1186 94. Kao DJ, Saeedi BJ, Kitzenberg D, Burney KM, Dobrinskikh E, Battista KD, et al. Intestinal
1187 Epithelial Ecto-5'-Nucleotidase (CD73) Regulates Intestinal Colonization and Infection by

1188 Nontyphoidal Salmonella. Infect Immun. 2017;85(10). Epub 2017/07/19. doi: 10.1128/IAI.01022-
1189 16. PubMed PMID: 28717030; PubMed Central PMCID: PMC5607412.
1190 95. Dho SH, Lim JC, Kim LK. Beyond the Role of CD55 as a Complement Component.
1191 Immune Netw. 2018;18(1):e11. Epub 2018/03/06. doi: 10.4110/in.2018.18.e11. PubMed PMID:
1192 29503741; PubMed Central PMCID: PMCPMC5833118.
1193 96. Huang Y, Qiao F, Abagyan R, Hazard S, Tomlinson S. Defining the CD59-C9 binding
1194 interaction. J Biol Chem. 2006;281(37):27398-404. Epub 2006/07/18. doi:
1195 10.1074/jbc.M603690200. PubMed PMID: 16844690.
1196 97. Lawrence DW, Bruyninckx WJ, Louis NA, Lublin DM, Stahl GL, Parkos CA, et al.
1197 Antiadhesive role of apical decay-accelerating factor (CD55) in human neutrophil transmigration
1198 across mucosal epithelia. The Journal of experimental medicine. 2003;198(7):999-1010. Epub
1199 2003/10/08. doi: 10.1084/jem.20030380. PubMed PMID: 14530374; PubMed Central PMCID:
1200 PMC2194216.
1201 98. Greene NG, Narciso AR, Filipe SR, Camilli A. Peptidoglycan Branched Stem Peptides
1202 Contribute to Streptococcus pneumoniae Virulence by Inhibiting Pneumolysin Release. PLoS
1203 pathogens. 2015;11(6):e1004996. Epub 2015/06/27. doi: 10.1371/journal.ppat.1004996.
1204 PubMed PMID: 26114646; PubMed Central PMCID: PMC4483231.
1205 99. Shainheit MG, Mule M, Camilli A. The core promoter of the capsule operon of
1206 Streptococcus pneumoniae is necessary for colonization and invasive disease. Infect Immun.
1207 2014;82(2):694-705. Epub 2014/01/31. doi: 10.1128/IAI.01289-13. PubMed PMID: 24478084;
1208 PubMed Central PMCID: PMC3911406.
1209 100. Yuste J, Khandavilli S, Ansari N, Muttardi K, Ismail L, Hyams C, et al. The effects of PspC
1210 on complement-mediated immunity to Streptococcus pneumoniae vary with strain background
1211 and capsular serotype. Infect Immun. 2010;78(1):283-92. Epub 2009/11/04. doi:
1212 10.1128/IAI.00541-09. PubMed PMID: 19884335; PubMed Central PMCID: PMC2798213.

1213 101. Price KE, Greene NG, Camilli A. Export requirements of pneumolysin in Streptococcus
1214 pneumoniae. J Bacteriol. 2012;194(14):3651-60. Epub 2012/05/09. doi: 10.1128/jb.00114-12.
1215 PubMed PMID: 22563048; PubMed Central PMCID: PMCPMC3393478.
1216 102. Herring SE, Mao S, Bhalla M, Tchalla EYI, Kramer JM, Bou Ghanem EN. Mitochondrial
1217 ROS production by neutrophils is required for host antimicrobial function against Streptococcus
1218 pneumoniae and is controlled by A2B adenosine receptor signaling. PLOS Pathogens.
1219 2022;18(11):e1010700. doi: 10.1371/journal.ppat.1010700.
1220 103. Bhalla M, Law D, Dowd GC, Ireton K. Host Serine/Threonine Kinases mTOR and Protein
1221 Kinase C-α Promote InlB-Mediated Entry of Listeria monocytogenes. Infection and immunity.
1222 2017;85(7):e00087-17. doi: 10.1128/IAI.00087-17. PubMed PMID: 28461391.
1223 104. Bhalla M, Law D, Dowd GC, Ireton K. Host Serine/Threonine Kinases mTOR and Protein
1224 Kinase C-alpha Promote InlB-Mediated Entry of Listeria monocytogenes. Infect Immun.
1225 2017;85(7). Epub 2017/05/04. doi: 10.1128/IAI.00087-17. PubMed PMID: 28461391; PubMed
1226 Central PMCID: PMCPMC5478960.
1227 105. Hirata T, Mishra SK, Nakamura S, Saito K, Motooka D, Takada Y, et al. Identification of a
1228 Golgi GPI-N-acetylgalactosamine transferase with tandem transmembrane regions in the
1229 catalytic domain. Nature Communications. 2018;9(1):405. doi: 10.1038/s41467-017-02799-0.
1230 106. Dowd GC, Bhalla M, Kean B, Thomas R, Ireton K. Role of Host Type IA Phosphoinositide
1231 3-Kinase Pathway Components in Invasin-Mediated Internalization of Yersinia enterocolitica.
1232 Infection and Immunity. 2016;84(6):1826-41. doi: doi:10.1128/IAI.00142-16.
1233 107. Yoshizaki H, Ohba Y, Kurokawa K, Itoh RE, Nakamura T, Mochizuki N, et al. Activity of
1234 Rho-family GTPases during cell division as visualized with FRET-based probes. J Cell Biol.
1235 2003;162(2):223-32. Epub 2003/07/16. doi: 10.1083/jcb.200212049. PubMed PMID: 12860967;
1236 PubMed Central PMCID: PMCPMC2172791.
1237 108. Itoh RE, Kurokawa K, Ohba Y, Yoshizaki H, Mochizuki N, Matsuda M. Activation of rac
1238 and cdc42 video imaged by fluorescent resonance energy transfer-based single-molecule probes

1239 in the membrane of living cells. Mol Cell Biol. 2002;22(18):6582-91. Epub 2002/08/23. doi:
1240 10.1128/mcb.22.18.6582-6591.2002. PubMed PMID: 12192056; PubMed Central PMCID:
1241 PMCPMC135619.

1242